

Selective Inference for Sparse Multitask Regression with Applications in Neuroimaging

Snigdha Panigrahi¹, Natasha Stewart¹, Chandra Sripada^{2,3}, and Elizaveta Levina¹

¹Department of Statistics, University of Michigan

²Department of Psychiatry, University of Michigan

³Department of Philosophy, University of Michigan

Multi-task learning is frequently used to model a set of related response variables from the same set of features, improving predictive performance and modeling accuracy relative to methods that handle each response variable separately. Despite the potential of multi-task learning to yield more powerful inference than single-task alternatives, prior work in this area has largely omitted uncertainty quantification. Our focus in this paper is a common multi-task problem in neuroimaging, where the goal is to understand the relationship between multiple cognitive task scores (or other subject-level assessments) and brain connectome data collected from imaging. We propose a framework for selective inference to address this problem, with the flexibility to: (i) jointly identify the relevant covariates for each task through a sparsity-inducing penalty, and (ii) conduct valid inference in a model based on the estimated sparsity structure. Our framework offers a new conditional procedure for inference, based on a refinement of the selection event that yields a tractable selection-adjusted likelihood. This gives an approximate system of estimating equations for maximum likelihood inference, solvable via a single convex optimization problem, and enables us to efficiently form confidence intervals with approximately the correct coverage. Applied to both simulated data and data from the Adolescent Cognitive Brain Development (ABCD) study, our selective inference methods yield tighter confidence intervals than commonly used alternatives, such as data splitting. We also demonstrate through simulations that multi-task learning with selective inference can more accurately recover true signals than single-task methods.

Keywords: Multi-task learning, multi-level Lasso, joint sparsity, post-selection inference, selective inference, neuroimaging, fMRI data

1 Introduction

Multi-task learning (MTL) is an important tool for studying related response variables that share a common set of predictors and potentially common patterns of dependence between the predictors and responses. In neuroimaging, researchers embrace the multi-task setting to jointly analyze imaging data and clinical assessments under a single regression framework. For example, MTL has been applied to study neurodegenerative disease patients over time (Zhou et al., 2013), identify important imaging predictors of schizophrenia using data from multiple study sites (Ma et al., 2018; Hu and Zeng, 2019), and predict cognitive profiles using multiple imaging modalities (Zu et al., 2016; Xiao et al., 2019). Relative to single-task methods, MTL algorithms are known to significantly improve prediction accuracy in these applications by accounting for the presence of shared information between the tasks. Many different MTL algorithms have been developed, including regression methods that impose inter-task dependence through shared sparsity or low-rank constraints on the multi-task regression coefficients; see Zhang and Yang (2021) and references therein for a thorough survey on the topic.

While there are many MTL algorithms for prediction, there are limited options for quantifying uncertainty in the estimated effects of the selected predictors. Few exceptions include Titsias and Lázaro-Gredilla (2011) and Gonçalves et al. (2019). Both papers recognize the need for greater focus on inference in MTL, proposing hierarchical Bayesian approaches to sparse MTL with uncertainty quantification through variational inference and posterior Gibbs sampling, respectively. The practicality of these methods is limited by the number of hyper-parameters that must be tuned, as well as the need to optimize several variational parameters in the former case and to employ computationally-intensive MCMC sampling methods in the latter case. More fundamentally, these Bayesian methods facilitate inference under the posterior model before examining data, while experts frequently wish to modify the model after exploring the data and obtaining initial results. In this paper, we develop a new set of techniques for uncertainty quantification in MTL through selective inference. Relative to other inference paradigms, selective inference offers the flexibility of choosing the model under which to conduct inference *after* examining the data. Classical inference procedures are, of course, rendered invalid when the model is selected only after observing the outcome of interest, and tools for selective inference provide a rigorous roadmap for overcoming this daunting challenge (Bi et al., 2020; Benjamini, 2020).

Selective inference has been studied extensively for single-task prediction algorithms. A common approach to selective inference, described by Fithian et al. (2017), accounts for bias from model selection by conditioning upon the chosen model. The inherent difficulty in this approach is characterizing the selection event in a sufficiently simple form to be conditioned upon. For models chosen based on the LASSO solution, Lee et al. (2016) developed the influential polyhedral method, reducing the

selection event to a series of affine inequalities in the response variable. Many different model selection events for a Gaussian response variable have subsequently been developed using a similar set of constraints, yielding tractable conditional distributions that can be used for inference (Suzumura et al., 2017; Liu et al., 2018; Taylor and Tibshirani, 2018; Zhao and Panigrahi, 2019; Tanizaki et al., 2020, among others). Despite the convenience of the polyhedral method, the resulting confidence intervals can have infinite expected length under Gaussian regression, formally established by Kivaranovic and Leeb (2018).

Applying the principles of conditional inference to a randomized problem, for example, by adding random noise to the response variable (Tian and Taylor, 2018) or by holding out some samples during selection—a technique called data carving (Fithian et al., 2017; Panigrahi, 2018), remedies the loss of inferential power and ensures bounded confidence intervals after selection. A randomized version of an existing selection algorithm can be obtained by introducing small perturbations at the time of model selection. Some amount of information will necessarily be available to conduct inference on the original data after marginalizing over the random noise, or randomization variable. Following the conditional approach, a selection-adjusted likelihood for the parameters in the chosen model then replaces the usual likelihood (ignoring selection). Under randomized versions of single-task algorithms such as the LASSO, Tian and Taylor (2018) obtained a pivot for each parameter in this likelihood after eliminating other (nuisance) parameters by conditioning on their corresponding sufficient statistics. More recently, Panigrahi and Taylor (2022) and Panigrahi et al. (2018, 2021) build upon the polyhedral method to describe an operational likelihood that permits the flexibility to conduct frequentist and Bayesian selective inference, using a prior in conjunction with the likelihood in the latter case.

The main motivation for our current work on multi-task selective inference is the data from the Adolescent Brain Cognitive Development (ABCD) study, an ongoing longitudinal study with 21 different research sites throughout the United States. Since the beginning of the study in 2015, over 10,000 children have been enrolled to help experts identify typical and atypical trajectories of brain development and their association with social, emotional, and cognitive functioning in adolescence (Jernigan et al., 2018; Hagler Jr et al., 2019). The study uses multiple modalities to track the participants’ brain development, including resting-state functional imaging, task functional imaging, and structural imaging. Various assessments are administered to measure the participants’ functioning in different areas, including a battery of cognitive tests based on the NIH Toolbox for the Assessment of Neurological and Behavioral Function. In our analysis, we consider the relationship between the subjects’ scores on 11 cognitive tasks and their resting-state fMRI connectivity data. Previously, Sripada et al. (2020, 2021) have successfully predicted the subjects’ performance on these tasks using features extracted from resting-state fMRI data, but the question of statistical inference in this setting has been

largely unaddressed. By applying our selective inference procedure to this data set, we are able to not only predict the subjects’ task scores but also quantify uncertainty in the selected models to address important scientific questions. As an example, selective inference allows us to test whether some neurological features have a significant association with performance across cognitive tasks and quantify the uncertainty in their estimated effects.

Our proposed procedure follows a two-stage protocol. In stage one, we use a randomized MTL algorithm with a sparsity-inducing penalty for joint model selection. Our algorithm is based on a common multiplicative parameterization where the multi-task regression coefficients are represented as the product of a task-specific coefficient and a common coefficient that is shared between tasks. This parameterization has been used for joint estimation in a number of penalized MTL algorithms (Bi et al., 2008; Lozano and Swirszcz, 2012; Wang et al., 2016). In stage two, we conduct selective inference in the model chosen from the estimated sparsity structure. The prevailing polyhedral methods for single-task prediction algorithms (Lee et al., 2016; Panigrahi and Taylor, 2022), however, do not generalize well to the multi-task setting. This is because the usual conditioning event for single-task prescriptions fails to admit a simple characterization when adapted to the setting of joint model selection. Remarkably, based on some shared information between the tasks, there is a partition of the conditioning event for our particular procedure that makes conditional inference feasible without being so fine as to sacrifice much power. We develop a new method for the multi-task setting, conditioning on this refinement of the selection event, and derive an easily-solvable system of estimating equations for approximate maximum likelihood inference. In contrast to the existing Bayesian proposals for inference within the MTL framework, our method only involves a single hyper-parameter and avoids the use of MCMC sampling methods for uncertainty estimation in the jointly selected models.

The rest of the paper is organized as follows. Section 2 explains our algorithm for estimating the shared sparsity structure, and Section 3 develops methods for MLE-based inference. We consider the empirical performance of our methods on simulated data in Section 4 and apply them to multi-task fMRI data from the ABCD study in Section 5.

2 Multi-Task Learning for Joint Model Selection

2.1 The Two-Stage Model Selection and Inference Protocol

For ease of presentation, we first review the two-stage protocol for model selection and subsequent valid, selective inference for the (single-task) randomized LASSO described in Panigrahi and Taylor (2022), before proceeding to the multi-task case. Suppose we observe (i) a predictor matrix $X \in \mathbb{R}^{n \times p}$ with fixed entries; (ii) a random response vector $y \sim N(\mu, \Sigma) \in \mathbb{R}^n$ for μ unknown and Σ known; and (iii) an independent randomization variable $\omega \sim N(0, \Omega) \in \mathbb{R}^p$ for a known covariance matrix

Ω . In the first stage, we identify a sparse linear model, working within a randomized framework. The support of the model is identified through a randomized LASSO regression. We estimate the regression coefficients, $\Theta \in \mathbb{R}^p$, by solving

$$\hat{\Theta} = \underset{\Theta}{\operatorname{argmin}} \mathcal{L}(\Theta; y, X, \omega) + \|\Lambda\Theta\|_1, \quad (1)$$

where $\Lambda \in \mathbb{R}^{p \times p}$ represents a diagonal matrix of feature-specific tuning parameters. The randomized loss $\mathcal{L}(\cdot; y, X, \omega)$ for the triplet y, X and ω is given by

$$\mathcal{L}(\Theta; y, X, \omega) = \frac{1}{2} \|y - X\Theta\|_2^2 - \omega'\Theta + \frac{\epsilon}{2} \|\Theta\|_2^2. \quad (2)$$

The ridge term in the loss function, with a small ϵ , is included to ensure convexity and hence the existence of an optimal solution. We use M' to denote the transpose of a matrix M . The estimated support set, $\hat{E} = \operatorname{Supp}(\hat{\Theta})$, is treated as random, reflecting the fact that different samples of y and ω will yield different active sets. Suppose we observe $\hat{E}(y, \omega) = E$ on our specific data. We use $|E|$ to denote the cardinality of set E and $X_E \in \mathbb{R}^{n \times |E|}$ to represent the restriction of X to the columns indexed by E .

After observing the active set E , we assume a linear model of the form $y \sim N(X_E\beta_E, \sigma^2\mathbf{I}_n)$, where σ is fixed and \mathbf{I}_n is the $n \times n$ identity matrix. This model is easy to work with, but there are other options for specifying a model based on the estimated active set. Post-selection inference affords us the flexibility to choose from a range of such models. For instance, the two-stage protocol we describe here can also be used for other linear models, such as those involving linear combinations of basis functions constructed from the active features.

In the second stage, we aim to construct $100(1 - \alpha)\%$ confidence intervals for the best linear coefficients,

$$\beta_E = \underset{\beta \in \mathbb{R}^{|E|}}{\operatorname{argmin}} \mathbb{E} [\|y - X_E\beta\|_2^2], \quad (3)$$

under the post-selection model. A conditional likelihood for β_E is obtained by conditioning upon the partition

$$\mathcal{P}_E = \{y \in \mathbb{R}^n, \omega \in \mathbb{R}^p : \hat{E}(y, \omega) = E\},$$

that contains all instances leading us to observe the estimated support set E . Letting $\rho(x; \mu, \Omega)$ be the multivariate normal density function with mean vector μ and covariance Ω , we can write this likelihood as

$$y | \hat{E} = E \propto \frac{\rho(y; X_E\beta_E, \sigma^2\mathbf{I}_n)}{\int_{\mathcal{P}_E} \rho(\tilde{y}; X_E\beta_E, \sigma^2\mathbf{I}_n) \cdot \rho(\tilde{\omega}; 0, \Omega) d\tilde{\omega} d\tilde{y}}. \quad (4)$$

The likelihood in (4) does not have a closed form since the normalizing constant is intractable. Instead, a tractable version of the likelihood function, called the selection-adjusted likelihood, is obtained by conditioning on a refined event,

$$\left\{\widehat{S}(y, \omega) = S\right\} \subseteq \left\{\widehat{E}(y, \omega) = E\right\},$$

that can be characterized by the polyhedral partition

$$\{y \in \mathbb{R}^n, \omega \in \mathbb{R}^p : Ay + B\omega \leq c\}$$

for fixed matrices A , B and c . For example, Lee et al. (2016) identify a polyhedral partition by conditioning further on the active signs of the LASSO solution, alongside the estimated support set E .

Approximate inference is then obtained by centering interval estimates around the maximum likelihood estimate (MLE) of the selection-adjusted likelihood, $\widehat{\beta}_E^{\text{MLE}}$, and using the observed Fisher information matrix, $\widehat{I}(\widehat{\beta}_E^{\text{MLE}})$, to estimate the variance. This yields post-selection confidence intervals for β_E of the form

$$\widehat{\beta}_{E,j}^{\text{MLE}} \pm z_{1-\alpha/2} \sqrt{\widehat{I}_{jj}^{-1}(\widehat{\beta}_E^{\text{MLE}})}, \quad j \in E;$$

where v_j is the j^{th} entry of the vector v , M_{ij} is the $(i, j)^{\text{th}}$ element of a matrix M , and z_q is the q^{th} quantile of the standard normal distribution.

2.2 An Objective Function with Shared Sparsity for MTL

We next set up the objective function in the multi-task setting. Suppose we have K regression tasks, with K distinct response variables and a common set of p predictors. For $k \in [K]$, let n_k denote the sample size available for task k , $y^{(k)} \in \mathbb{R}^{n_k}$ denote the response vector for the k^{th} task, and $X^{(k)} \in \mathbb{R}^{n_k \times p}$ denote the corresponding predictor matrix. Let $N = n_1 + \dots + n_K$. We assume that the predictors in each task have been centered and do not include intercept terms in the regression. Consistent with the two-stage procedure described in Section 2.1, we introduce a randomization variable for each task. Let $\omega^{(k)} \in \mathbb{R}^p$ denote a Gaussian randomization variable such that (i) $\omega^{(k)} \sim \mathcal{N}(0, \Omega^{(k)})$ for $k \in [K]$; (ii) $\omega^{(k)}$ is independent of $\omega^{(k')}$ for all $k' \neq k$; and (iii) $\omega^{(k)}$ is independent of $y^{(k')}$ for all $k' \in [K]$.

For each task, we assume that the set of non-zero coefficients is sparse and use penalized multi-task regression to identify the relevant features. We impose a specific inter-task structure on the joint regression by assuming that the coefficients $\Theta^{(1)}, \dots, \Theta^{(K)} \in \mathbb{R}^p$ can be represented as the product of a common parameter that is shared between all tasks and a task-specific parameter that is unique to an

individual task; namely,

$$\Theta_j^{(k)} = \tau_j \gamma_j^{(k)}, \text{ for } j \in [p], k \in [K]. \quad (5)$$

To avoid a sign ambiguity, we take $\tau_j \geq 0$ for $j \in [p]$. We do not impose any further constraints to ensure that the two components, τ_j and $\gamma_j^{(k)}$, are each identifiable since our interest lies in estimating the sparsity structure of their product. Note that τ_j determines the sparsity at the global level as $\tau_j = 0$ implies that $\Theta_j^{(k)} = 0$ for all $k \in [K]$. The parameter $\gamma_j^{(k)}$ controls task-specific sparsity, with $\gamma_j^{(k)} = 0$ indicating that $\Theta_j^{(k)} = 0$ for task k .

We proceed to fit a sparse model by minimizing the penalized objective function

$$\sum_{k=1}^K \mathcal{L}(\Theta^{(k)}; y^{(k)}, X^{(k)}, \omega^{(k)}) + \eta_1 \sum_{j=1}^p \tau_j + \eta_2 \sum_{j=1}^p \sum_{k=1}^K |\gamma_j^{(k)}|, \quad (6)$$

subject to the constraint $\tau_j \geq 0$ for $j \in [p]$. The minimizers $\hat{\tau} \in \mathbb{R}^p$, $\hat{\gamma}^{(k)} \in \mathbb{R}^p$ will clearly both be sparse due to the ℓ_1 penalties in the objective function. To optimize the objective (6), we note that its solution will yield coefficients $\Theta^{(k)}$ for $k \in [K]$ that could be obtained from an equivalent formulation

$$\underset{\{\Theta_j^{(k)}\}_{j \in [p], k \in [K]}}{\operatorname{argmin}} \sum_{k=1}^K \mathcal{L}(\Theta^{(k)}; y^{(k)}, X^{(k)}, \omega^{(k)}) + 2\lambda \sum_{j=1}^p \left\{ \sum_{k=1}^K |\Theta_j^{(k)}| \right\}^{1/2}, \quad (7)$$

where $\lambda = \sqrt{\eta_1 \eta_2}$. This equivalence was established in previous work; see, e.g., [Guo et al. \(2011\)](#) and [Lozano and Swirszcz \(2012\)](#).

Following the approach of [Guo et al. \(2011\)](#) and [Zou and Li \(2008\)](#), we use an iterative local linear approximation to the penalty term in (7), centered at the value at the previous iteration:

$$2 \left\{ \sum_{k=1}^K |\Theta_j^{(k)}| \right\}^{1/2} \sim c^{(t)} + \sum_{k=1}^K \frac{|\Theta_j^{(k)}|}{\sqrt{\sum_{k=1}^K |(\hat{\Theta}_j^{(k)})^{(t)}|}}.$$

The constant $c^{(t)}$ depends only on the previous iterate and can be ignored in the corresponding optimization problem. With this approximation, the multi-task objective conveniently decouples by task. The successive estimates of the regression coefficients can be computed by solving a LASSO problem separately for each of the K tasks, dependent on the previous iterate only through the penalty weights

$$\lambda_j^{(t+1)} = \min \left\{ \lambda_0, \lambda \cdot \left(\sum_{k=1}^K |(\hat{\Theta}_j^{(k)})^{(t)}| \right)^{-\frac{1}{2}} \right\}, \quad j \in [p].$$

Here, λ_0 is a pre-specified small positive constant used for numerical stability, and λ is a tuning parameter. The iterative procedure is summarized in Algorithm 1.

Upon convergence of Algorithm 1, we obtain

$$\hat{E}_k = \text{Supp}(\hat{\Theta}^{(k)}) = E_k, \text{ for } k \in [K]. \quad (8)$$

Let the cardinality of $E_k \subseteq [p]$ be equal to q_k , and let $q = q_1 + \dots + q_K$.

Algorithm 1 Estimating Shared Sparsity

```

1: for  $k = 1, \dots, K$  do
2:   Initialize  $(\hat{\Theta}^{(k)})^{(0)} = \underset{\Theta^{(k)}}{\text{argmin}} \left( \mathcal{L}(\Theta^{(k)}; y^{(k)}, X^{(k)}, \omega^{(k)}) + \lambda \sum_{j=1}^p |\Theta_j^{(k)}| \right)$ 
3: end for
4: procedure ITERATE UNTIL CONVERGENCE
5:   Let  $t = 0$ 
6:   while convergence  $<$  tol do
7:     for  $j = 1, \dots, p$  do
8:        $\lambda_j^{(t+1)} = \min \left\{ \lambda_0, \lambda \cdot \left( \sum_{k=1}^K |(\hat{\Theta}_j^{(k)})^{(t)}| \right)^{-\frac{1}{2}} \right\}$ 
9:     end for
10:    for  $k = 1, \dots, K$  do
11:      LASSO:
12:      Solve  $(\hat{\Theta}^{(k)})^{(t+1)} = \underset{\Theta^{(k)}}{\text{argmin}} \left( \mathcal{L}(\Theta^{(k)}; y^{(k)}, X^{(k)}, \omega^{(k)}) + \sum_{j=1}^p \lambda_j^{(t+1)} |\Theta_j^{(k)}| \right)$ 
13:    end for
14:     $t = t + 1$ 
15:  end while
16: end procedure

```

3 Maximum Likelihood Inference Post MTL

Next, we proceed to specify a model with the sparsity structure estimated through (6) and estimate uncertainty in the effects of selected predictors with respect to this model. We restrict our search to linear models of the form

$$y^{(k)} = X_{E_k}^{(k)} \beta_{E_k}^{(k)} + \varepsilon_k \text{ for } k \in [K], \quad (9)$$

where ε_k is a vector of errors of length n_k with mean 0 and variance σ_k^2 . We assume errors are independent across samples and across tasks. We fit this model by maximizing the corresponding normal likelihood, which can be viewed as a general M -estimation procedure. For the inference step, the post-selection confidence intervals for $\beta_{E_k}^{(k)}$ will be based on the normal assumption for the error distribution.

3.1 Some preliminaries

Without loss of generality, we can reorder each predictor matrix and randomization instance to have the active components precede the inactive components:

$$X^{(k)} = \begin{bmatrix} X_{E_k}^{(k)} & X_{-E_k}^{(k)} \end{bmatrix}, \quad \omega^{(k)} = \begin{pmatrix} \omega_{E_k}^{(k)} \\ \omega_{-E_k}^{(k)} \end{pmatrix},$$

where $-A$ denotes the complement of set A . For each predictor $j \in [p]$, we use \tilde{j}_k to denote the index of this predictor in task k after the permutation. Let $b^{(k)} \in \mathbb{R}^{q_k}$ denote the absolute values of the estimated non-zero multi-task regression coefficients for task $k \in [K]$ under this permutation, i.e.,

$$b_{\tilde{j}_k}^{(k)} = |\hat{\Theta}_j^{(k)}| \text{ whenever } |\hat{\Theta}_j^{(k)}| \neq 0.$$

We let $s^{(k)} \in \mathbb{R}^{q_k}$ and $u^{(k)} \in \mathbb{R}^{p-q_k}$ represent the active and inactive components of the subgradient vector of the ℓ_1 -norm for the multi-task regression coefficients when evaluated at the solution, i.e.,

$$\begin{pmatrix} s^{(k)'} & u^{(k)'} \end{pmatrix}' = \mathcal{D}_{\hat{\Theta}} \left\| \begin{pmatrix} \Theta_{E_k}^{(k)'} & \Theta_{-E_k}^{(k)'} \end{pmatrix}' \right\|_1 \text{ for } k \in [K].$$

Note that the vector $s^{(k)}$ gives the signs of the active multi-task coefficients for the k^{th} task, and $u^{(k)}$ satisfies $\|u^{(k)}\|_\infty \leq 1$.

We next introduce some notation to account for information shared across tasks. Suppose, there are r predictors, j_1, \dots, j_r , that are active in one or more tasks. Define $\Gamma \in \mathbb{R}^r$ by

$$\Gamma^{(j)} = \sum_{k=1}^K |\hat{\Theta}_j^{(k)}| \text{ for } j \in \{j_1, \dots, j_r\}$$

A boldface capital letter is used to denote the vector or set that results from stacking the quantities corresponding to the same letter. We collect these notations in Table 1.

Let

$$\kappa(j) = \{k : |\hat{\Theta}_j^{(k)}| \neq 0\}$$

be the tasks where predictor j is active, with $d_j = |\kappa(j)|$ and elements $\kappa_1 < \dots < \kappa_{d_j}$ arranged in increasing order. For the active predictors j_1, \dots, j_r , we define $v^{(j)}$ to be a vector representing the first $(d_j - 1)$ corresponding coefficients:

$$v^{(j)} = \left(|\hat{\Theta}_j^{(\kappa_1)}| \quad \dots \quad |\hat{\Theta}_j^{(\kappa_{d_j-1})}| \right)' \text{ for } j \in \{j_1, \dots, j_r\}$$

Symbol	Definition	Symbol	Definition
\mathbf{Y}	$\left(y^{(1)'} \dots y^{(K)'}\right)'$	\mathbf{S}	$\left(s^{(1)'} \dots s^{(K)'}\right)'$
\mathbf{W}	$\left(\omega^{(1)'} \dots \omega^{(K)'}\right)'$	\mathbf{U}	$\left(u^{(1)'} \dots u^{(K)'}\right)'$
\mathbf{E}	$\{E_1, \dots, E_k\}$	$\mathbf{\Lambda}$	$\left(\Lambda^{(1)'} \dots \Lambda^{(K)'}\right)'$
$\beta_{\mathbf{E}}$	$\left(\beta_{E_1}^{(1)'} \dots \beta_{E_k}^{(K)'}\right)'$	$\mathbf{\Gamma}$	$\left(\Gamma^{(j_1)} \dots \Gamma^{(j_r)}\right)'$
\mathbf{B}	$\left(b^{(1)'} \dots b^{(K)'}\right)'$	\mathbf{V}	$\left(v^{(j_1)'} \dots v^{(j_r)'}\right)'$

Table 1: Notation for stacked quantities

The vector $v^{(j)}$ collects the absolute value of the non-zero coefficients for predictor j across tasks, excluding the coefficient for the last task where predictor j is non-zero. For most predictors in the active set, we expect that $d_j \geq 2$ due to the shared sparsity across tasks; however, if we estimate $d_j = 1$, then $v^{(j)}$ is empty and can be disregarded. Note that there is a bijective mapping between \mathbf{B} and $(\mathbf{V}, \mathbf{\Gamma})$. We introduce a matrix $D \in \mathbb{R}^{r \times (q-r)}$ to record which elements of \mathbf{V} correspond to each of the r active predictors, with rows given by

$$D_i = \left(\mathbf{0}'_{(d_{j_1}-1)} \quad \dots \quad \mathbf{1}'_{(d_{j_i}-1)} \quad \dots \quad \mathbf{0}'_{(d_{j_r}-1)} \right) \quad \text{for } i \in [r].$$

For some permutation matrix $\mathcal{A} \in \mathbb{R}^{q \times q}$, the relationship between \mathbf{B} and $(\mathbf{V}, \mathbf{\Gamma})$ is given by

$$\mathbf{B} = \mathcal{A} \begin{pmatrix} \mathbf{V} \\ \mathbf{\Gamma} - D\mathbf{V} \end{pmatrix}.$$

Let the matrix $H \in \mathbb{R}^{q \times (q-r)}$ and the vector $g \in \mathbb{R}^q$ be given by:

$$H = \begin{pmatrix} \mathbf{I}_{(q-r)} \\ -D \end{pmatrix} \quad g = \begin{pmatrix} \mathbf{0}_{(q-r)} \\ -\mathbf{\Gamma} \end{pmatrix}$$

To enforce the q linear inequalities given by $Hv \geq g$, we use the following barrier function:

$$\phi_{H,g}(v) = \begin{cases} \sum_{j=1}^q \log \left(1 + \frac{1}{H_j v - g_j} \right) & \text{if } Hv > g \\ \infty & \text{else.} \end{cases},$$

where H_j is the j^{th} row of H and g_j is the j^{th} component of g .

3.2 Estimating Equations for Approximate MLE-Based Inference

A natural starting point for selective inference in the multi-task setting is the law for \mathbf{Y} , conditioning on the event

$$\{\widehat{\mathbf{E}} = \mathbf{E}, \widehat{\mathbf{S}} = \mathbf{S}\}. \quad (10)$$

This conditional prescription results in practical selective inference procedures for other ℓ_1 -regularized algorithms by constraining the response to fall within a polyhedral partition of the sample space. Consider, for example, the randomized LASSO procedure described in section 2.1. The event (10), characterized through the K.K.T. conditions, induces an affine map from the randomization variable ω to the absolute coefficients b and subgradient u at the optimal solution. Under this transformation, the Jacobian contributes only a proportionality constant to the conditional law of (y, b, u) given (10), yielding a multivariate Gaussian distribution truncated to a polyhedral partition. The distribution for y that results from conditioning upon u and marginalizing over b can be used to facilitate approximate MLE-based inference (Panigrahi and Taylor, 2022).

Unfortunately, this conditional prescription does not generalize well to the MTL setting. Note that the stationary map for the model selection procedure in Algorithm 1, given \mathbf{E} and \mathbf{S} , induces the following transformation:

$$\mathbf{W} = \begin{pmatrix} \pi^{(1)}(b^{(1)}, u^{(1)}) & \pi^{(2)}(b^{(2)}, u^{(2)}) & \dots & \pi^{(K)}(b^{(K)}, u^{(K)}) \end{pmatrix},$$

where

$$\begin{aligned} \pi(b^{(k)}, u^{(k)}) = & -X^{(k)'} y^{(k)} + \begin{bmatrix} (X_{E_k}^{(k)})' X_{E_k}^{(k)} + \epsilon \cdot \mathbf{I}_{q_k} \\ (X_{-E_k}^{(k)})' X_{E_k}^{(k)} \end{bmatrix} \text{Diag}(s^{(k)}) b^{(k)} \\ & + \text{Diag}(\Lambda^{(k)}) \begin{pmatrix} s^{(k)} \\ u^{(k)} \end{pmatrix}, \end{aligned} \quad (11)$$

$$\Lambda_{j_k}^{(k)} = \min \left\{ \lambda_0, \lambda \cdot \left(\sum_{k=1}^K |(\widehat{\Theta}_j^{(k)})| \right)^{-\frac{1}{2}} \right\}, \quad j \in [p].$$

Observe that this transformation is non-affine since the penalty term is now related to the solution. The change-of-variables Jacobian, given in the Proposition 1 of the Appendix, is a complicated function of (\mathbf{B}, \mathbf{U}) . Deriving estimating equations for maximum-likelihood inference using the law of $(\mathbf{Y}, \mathbf{B}, \mathbf{U})$ conditional upon (10) would require closed form expressions for the partial derivatives of the Jacobian, which are not available. For completeness sake, we provide the likelihood based on this conditional law in Proposition 2 under the Appendix.

Instead, we propose a different approach that can remarkably bypass the intractable Jacobian and

avoid cumbersome numerical integrations to easily facilitate maximum likelihood inference. We will work with an exact selection-adjusted likelihood, derived by conditioning on a refined partition of the event in (10):

$$\widehat{\mathbf{E}} = \mathbf{E}, \widehat{\mathbf{S}} = \mathbf{S}, \widehat{\mathbf{\Gamma}} = \mathbf{\Gamma}, \widehat{\mathbf{U}} = \mathbf{U}. \quad (12)$$

We form our estimating equations for maximum likelihood inference in terms of the least squares estimator based on the selected predictors for each task,

$$\widehat{\beta}_{E_k}^{(k)} = (X_{E_k}^{(k)})^\dagger y^{(k)}. \quad (13)$$

Note that the estimator in (13) is the naive MLE that we would have used if the sets E_k were specified before looking at the data. Dependent on $X^{(k)'} y^{(k)}$, the event of selection also relies on

$$\widehat{\beta}_\perp^{(k)} = (X^{(k)})' \left(\mathbf{I}_{n_k} - X_{E_k}^{(k)} (X_{E_k}^{(k)})^\dagger \right) y^{(k)},$$

the ancillary statistic we obtain through a projection of the response onto the subspace orthogonal to the span of the selected predictors $X_{E_k}^{(k)}$.

Lemma 3.1 first identifies an equivalent representation for the refined conditioning event in terms of \mathbf{V} , $\mathbf{\Gamma}$ and \mathbf{U} that we observe after solving the MTL Algorithm 1; please see Section 3.1 for a complete list of definitions.

Lemma 3.1 *Suppose \mathbf{V} , $\mathbf{\Gamma}$ are defined as above. Then the event (12) is equivalent to the event*

$$\mathbf{V} > \mathbf{0}, \widehat{\mathbf{\Gamma}} = \mathbf{\Gamma}, \mathbf{\Gamma} - D\mathbf{V} > \mathbf{0}, \widehat{\mathbf{U}} = \mathbf{U}.$$

The proof can be found in the Appendix. Consider the bijective mapping $\Psi_{\mathcal{A}} : \mathbb{R}^{K \cdot p} \rightarrow \mathbb{R}^{K \cdot p}$ such that

$$\begin{pmatrix} \mathbf{B}' & \mathbf{U}' \end{pmatrix}' = \Psi_{\mathcal{A}} \begin{pmatrix} \mathbf{V} & \mathbf{\Gamma} & \mathbf{U} \end{pmatrix} = \text{Diag}(\mathcal{A}, \mathbf{I}_{(Kp - q)}) \begin{pmatrix} \mathbf{V}' & (\mathbf{\Gamma} - D\mathbf{V})' & \mathbf{U}' \end{pmatrix}'.$$

Applying a change of variables via the composite mapping,

$$\mathbf{W} \xrightarrow{(\Pi_{\mathbf{X}'\mathbf{Y}} \circ \Psi_{\mathcal{A}})^{-1}} \begin{pmatrix} \mathbf{V} & \mathbf{\Gamma} & \mathbf{U} \end{pmatrix}, \quad (14)$$

we obtain an exact selection-adjusted likelihood in Theorem 3.2 after conditioning on the event in (12). The alternate characterization for the refined conditioning event in terms of the new variables \mathbf{V} , $\mathbf{\Gamma}$ and \mathbf{U} yields a selection-adjusted likelihood function that no longer involves the Jacobian, the term which previously hindered our attempts to solve the estimating equations. The normalizing constant

for our refined conditioning event is simply a Gaussian integral over a support set that is characterized by exactly q linear inequalities.

Theorem 3.2 *Consider the model in (9). The likelihood obtained from the law of the least squares estimates based on $\left\{X_{E_k}^{(k)}, y^{(k)}\right\}_{k=1}^K$ after conditioning upon the event in Lemma 3.1 is given by*

$$\left(\int \rho(\tilde{\beta}; L\beta_E + m, \Sigma) \cdot \rho(\tilde{V}; P\tilde{\beta} + q, \Delta) \cdot 1(H\tilde{V} \geq g) d\tilde{V} d\tilde{\beta} \right)^{-1} \cdot \rho(\hat{\beta}_E; L\beta_E + m, \Sigma).$$

Expressions for the matrices L , m , Σ , P , q , and Δ are provided in the Appendix. Taking a further step towards developing an easily solvable system of estimating equations for the MLE and the observed Fisher information matrix, $\hat{\mathbf{l}}(\hat{\beta}_E^{\text{MLE}})$, we bypass the integration in the normalizer, simply approximating it with the mode of the integrand in the selection region. That is,

$$\begin{aligned} & \log \int \rho(\tilde{\beta}; L\beta_E + m, \Sigma) \cdot \rho(\tilde{V}; P\tilde{\beta} + q, \Delta) \cdot 1(H\tilde{V} \geq g) d\tilde{V} d\tilde{\beta} \\ & \approx - \inf_{\tilde{\beta}, \tilde{V}} \left\{ \frac{1}{2} (\tilde{\beta} - L\beta_E - m)' \Sigma^{-1} (\tilde{\beta} - L\beta_E - m) \right. \\ & \quad \left. + \frac{1}{2} (\tilde{V} - P\tilde{\beta} - q)' \Delta^{-1} (\tilde{V} - P\tilde{\beta} - q) + \phi_{H,g}(\tilde{V}) \right\} \end{aligned} \quad (15)$$

ignoring an additive constant. This approximation in (15) then lends itself towards tractable equations for the selective MLE $\hat{\beta}_E^{\text{MLE}}$ and the observed Fisher information matrix, $\hat{\mathbf{l}}^{-1}$, given in Theorem 3.3.

Theorem 3.3 *Under the modeling assumptions in Theorem 3.2, the approximate selective MLE and observed information matrix satisfy the following system of estimating equations.*

$$\begin{aligned} \hat{\beta}_E^{\text{MLE}} &= L^{-1} \hat{\beta}_E + L^{-1} \Sigma P' \Delta^{-1} (P \hat{\beta}_E + q - \hat{\mathbf{V}}) - L^{-1} m, \\ \hat{\mathbf{l}}^{-1} &= L^{-1} \Sigma L'^{-1} + L^{-1} \Sigma \left(P' \Delta^{-1} P - P' \Delta^{-1} \left(\Delta^{-1} + \nabla^2 \phi_{H,g}(\hat{\mathbf{V}}) \right)^{-1} \Delta^{-1} P \right) \Sigma L'^{-1}, \end{aligned}$$

where $\hat{\mathbf{V}}$ is obtained from solving

$$\hat{\mathbf{V}} = \underset{\tilde{V}}{\operatorname{argmin}} \frac{1}{2} (\tilde{V} - P \hat{\beta}_E - q)' \Delta^{-1} (\tilde{V} - P \hat{\beta}_E - q) + \phi_{H,g}(\tilde{V}). \quad (16)$$

With these estimators for the approximate MLE and the observed Fisher information matrix, it is now possible to use maximum likelihood inference to form $100 \cdot (1 - \alpha)\%$ confidence intervals for the parameters within the MTL model (9). Algorithm 2 summarizes our procedure for post-MTL inference by reusing the same data.

Algorithm 2 Multi-Task Model Selection and Inference

17: Record the values for $\widehat{\mathbf{E}}, \widehat{\mathbf{S}}, \widehat{\mathbf{\Gamma}},$ and $\widehat{\mathbf{U}}$ at convergence of Algorithm 1
18: From the estimated sparsity structure, compute $\widehat{\beta}_{E_k}^{(k)}$ and $\widehat{\beta}_{\perp}^{(k)}$ for $k \in [K]$
19: Specify a significance level α
20: Compute $P, q,$ and Δ
21: Optimize (16) with gradient descent to compute $\widehat{\mathbf{V}}$
22: Compute the matrices L, m, Σ
23: **procedure** MAXIMUM LIKELIHOOD INFERENCE
24: Find $\widehat{\beta}_{\mathbf{E}}^{\text{MLE}}$ and $\widehat{\mathbf{I}}^{-1}$ based on the estimating equations in Theorem 3.3
25: **for** $j \in \{1, \dots, q\}$ **do**
26: Compute interval $\widehat{\beta}_{\mathbf{E},j}^{\text{MLE}} \pm z_{1-\alpha/2} \sqrt{\widehat{\mathbf{I}}_{jj}^{-1}(\widehat{\beta}_{\mathbf{E}}^{\text{MLE}})}$
27: **end for**
28: **end procedure**

4 Empirical Results

We empirically investigate the efficacy of our methods in recovering signals and estimating their strengths by simulating multi-task datasets with varying degrees of shared sparsity. We will compare the following methods:

1. **Naive:** Select an MTL model through the usual multi-task Lasso algorithm without a randomization term, and conduct inference without accounting for any selection bias.
2. **Data Splitting (DS(s)):** Divide the training data into two parts, using $\lceil sn_k \rceil$ samples from each task $k \in [K]$ for model selection with the usual multi-task algorithm, and reserve the rest for inference about the selected predictors.
3. **LASSO(v) + SI:** Apply the randomized LASSO separately to each task using independent randomization variables, $\omega^{(k)} \sim N(0, v^2 \sigma^2 \cdot \mathbf{I})$ for $k \in [K]$, and proceed with selective inference (SI) using the maximum likelihood approach of Panigrahi and Taylor (2022).
4. **MTL(v) + SI:** Our proposed approach. Use Algorithm 1 to select an MTL model based on K independent Gaussian randomization variables, $\omega^{(k)} \sim N(0, v^2 \sigma^2 \cdot \mathbf{I})$ for $k \in [K]$, and construct SI confidence intervals by Algorithm 2.

To ensure a fair comparison, each method is tuned separately on an equal-sized validation set. We select methods that use comparable amounts of information for model selection based on a rough equivalence between data splitting and a randomization variable with variation parameter

$$v = \sqrt{\frac{1-s}{s}}$$

for a Gaussian response; see (Panigrahi et al., 2021). The two comparable pairs we consider are MTL(0.7) vs. DS (0.67) and MTL(1.0) vs. DS(0.5).

4.1 Experimental settings

We generate the data from the linear regression model (9) with noise variance equal to 1. For each task k , we generate the entries of the $n_k \times p$ design matrix $X^{(k)}$ by taking n_k samples from a p -dimensional Gaussian distribution $N(0_p, \mathcal{T}(\rho))$ with

$$\mathcal{T}_{ij}(\rho) = \begin{cases} \rho & \text{if } i \neq j \\ 1 & \text{otherwise.} \end{cases}$$

The structure of the coefficients $\beta \in \mathbb{R}^{p \times K}$ in the MTL model is controlled by two parameters, the global sparsity level s_G and the task-specific sparsity level s_T , both numbers between 0 and 1. To specify the coefficients:

1. First, choose $\lceil s_G p \rceil$ predictors at random to be globally null for every task, and set the corresponding rows of β to zero.
2. For the remaining set of globally active predictors, set $\lceil s_T K \rceil$ randomly selected entries of each row of β to zero, independently for each task.
3. For each predictor $j \in [p]$, specify the corresponding non-zero coefficients by sampling without replacement from an equally-spaced sequence of values covering the interval

$$[\sqrt{2 \log(p)}, \sqrt{6 \log(p)}].$$

Randomly assign each coefficient a sign drawn from $\{-1, 1\}$.

Note that a task-level sparsity value $s_T = 0$ would mean that all tasks share the same active predictors, and the higher s_T is, the more heterogeneity in the predictors used by each task. Overall, the expected fraction of all of the $K \times p$ coefficients set to zero is $s_G \times s_T$.

We design three sets of examples to study the effects of (1) varying the heterogeneity in predictors across tasks by varying task sparsity s_T at a fixed value of global sparsity s_G ; (2) varying global sparsity s_G at a fixed value of task sparsity s_T ; and (3) varying the number of predictors p , fixing s_T and the total number of active predictors. In all of the examples, we set $n = 500$, $K = 5$, $\rho = 0.3$, and $\alpha = 0.1$. For scenario (1), we additionally fix $p = 100$, $s_G = 0.9$, and vary task sparsity s_T from 0 to

0.6. The signal-to-noise ratio per task, defined as

$$\text{SNR} = \frac{\beta^{(k)'} \mathcal{T}(\rho) \beta^{(k)}}{n_k \sigma^2},$$

averages around 0.1 across tasks in the first set of experiments. For scenario (2), we fix $p = 100$, $s_T = 0.2$, and vary s_G between 0.8 and 0.95. The average SNR per task is around 0.5 for global sparsity of 80 percent and decreases with increasing global sparsity. In both of the first two scenarios, we perform 100 replications. The optimal tuning parameter for each method is the value on the λ -path that yields the lowest average MSE on the validation set across iterations, and the results are reported at that tuning parameter value for all 100 iterates. For setting (3), we fix $t_S = 0.2$, set s_G so that the expected number of active predictors per task is 10, and vary p between 100 and 1000. The average SNR-per task increases to around 2.5 for the highest-dimensional setting to compensate for the added complexity. Due to the computational cost required to tune the model for larger p , we use 10 auxiliary iterations to choose tuning parameters and then use these parameters for the 100 iterations we report.

The following metrics are used to evaluate performance. First, we compute the empirical coverage rate (CR) of the post-selection intervals for non-zero coefficients, defined by

$$\text{CR} = 1 - \frac{|\{j \in \hat{\mathbf{E}} : \beta_{\mathbf{E},j} \notin C_{\hat{\mathbf{E}},j}\}|}{\max(|\hat{\mathbf{E}}|, 1)}.$$

This rate is further averaged over replications. We assess power of post-selection inference by reporting the lengths of the confidence intervals for the selected parameters. Finally, we measure the overall accuracy of model selection and subsequent inference by the F1 score, defined as

$$\text{F1} = 2 \cdot \frac{\text{precision} \times \text{recall}}{\text{precision} + \text{recall}}.$$

For our purposes, precision is the proportion of truly active predictors among those that were both selected into the model and deemed significant after inference, where significance means that the confidence interval for the corresponding effect did not cover zero. Recall is the proportion of all truly active predictors that were both selected into the model and deemed significant after inference. That is,

$$\text{Precision} = \frac{|\mathbf{E}_0 \cap \{j \in \hat{\mathbf{E}} : 0 \notin C_{\hat{\mathbf{E}},j}\}|}{|\{j \in \hat{\mathbf{E}} : 0 \notin C_{\hat{\mathbf{E}},j}\}|}; \text{Recall} = \frac{|\mathbf{E}_0 \cap \{j \in \hat{\mathbf{E}} : 0 \notin C_{\hat{\mathbf{E}},j}\}|}{|\mathbf{E}_0|},$$

where \mathbf{E}_0 is the set of true active predictors.

4.2 Experimental results

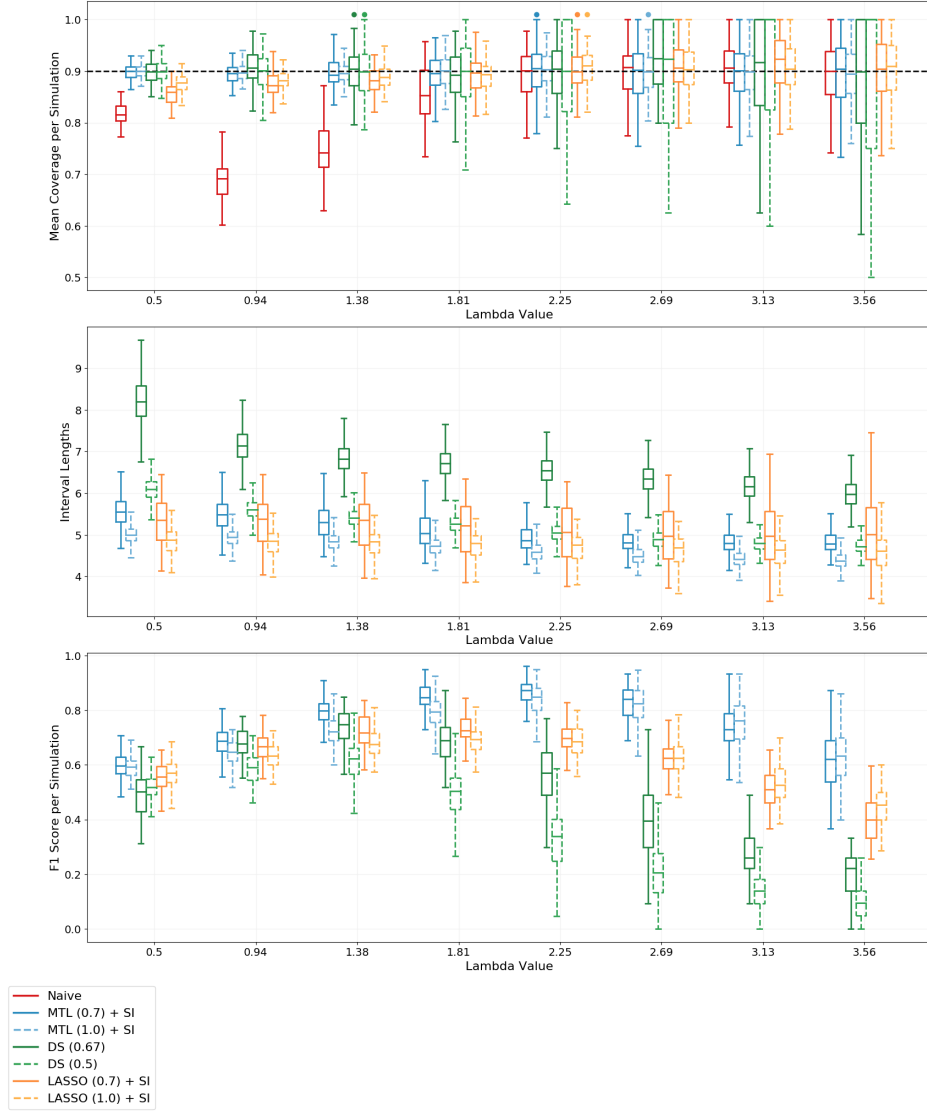


Figure 1: Coverage, length, and accuracy along the path of λ for the setting $s_G = 0.9$, $s_T = 0.2$, and $p = 100$. The solid and dashed lines are used to group methods that use a comparable amount of information for model selection; randomization parameters $v = 0.70$ and $v = 1$ are comparable to data splitting with $s = 0.67$ and $s = 0.50$, respectively.

We start from examining the results over the entire path of the tuning parameter λ . Figure 1 shows the coverage, interval length, and F1 score for a range of values of λ for the setting $s_G = 0.9$, $s_T = 0.2$, and $p = 100$. The distribution of coverage for the “naive” method underscores the dangers of ignoring model selection bias, with much higher variability in coverage than the post-selection methods. Reassuringly, all the post-selection methods achieve the nominal coverage rate of 0.9, regardless of

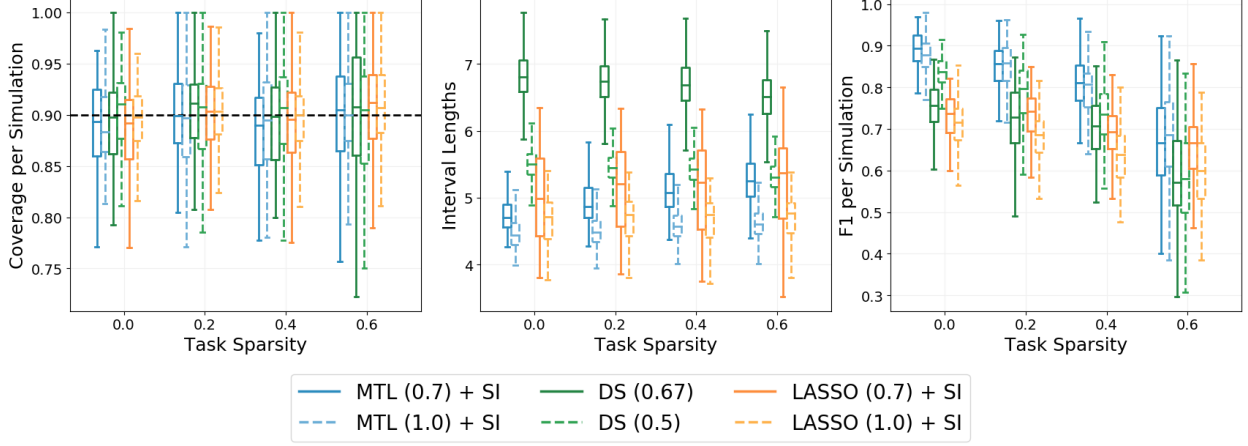


Figure 2: Results for 100 replications as a function of task sparsity s_T , fixing global sparsity $s_G = 0.9$ and $p = 100$. Top: coverage; middle: interval length; bottom: F1 score.

the choice of tuning parameter and subsequent quality of model selected. The interval lengths along the path of λ show that the methods based on randomization consistently produce tighter confidence intervals than the equivalent data splitting approach. However, it is not possible to directly compare the accuracy of inference from each method at the same, fixed value of the tuning parameter since the quality of the model selected by each method varies considerably along with λ . The F1 score, for example, achieves its best value at different points along the path for different methods. The colored dots in the top panel of Figure 2 show the value of λ that yielded the lowest mean squared error (MSE) on the holdout data set. From this point on, we will compare methods using the optimal value of the tuning parameter, chosen by minimizing the MSE on the validation data, for each method.

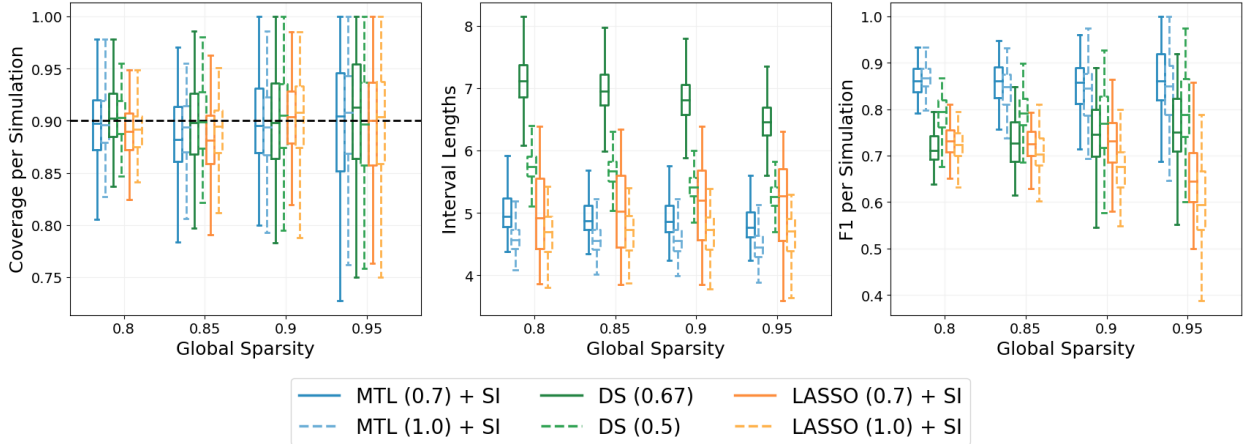


Figure 3: Results for 100 replications as a function of global sparsity s_G , fixing task sparsity $s_T = 0.2$ and $p = 100$. Left: coverage; middle: interval length; right: F1 score.

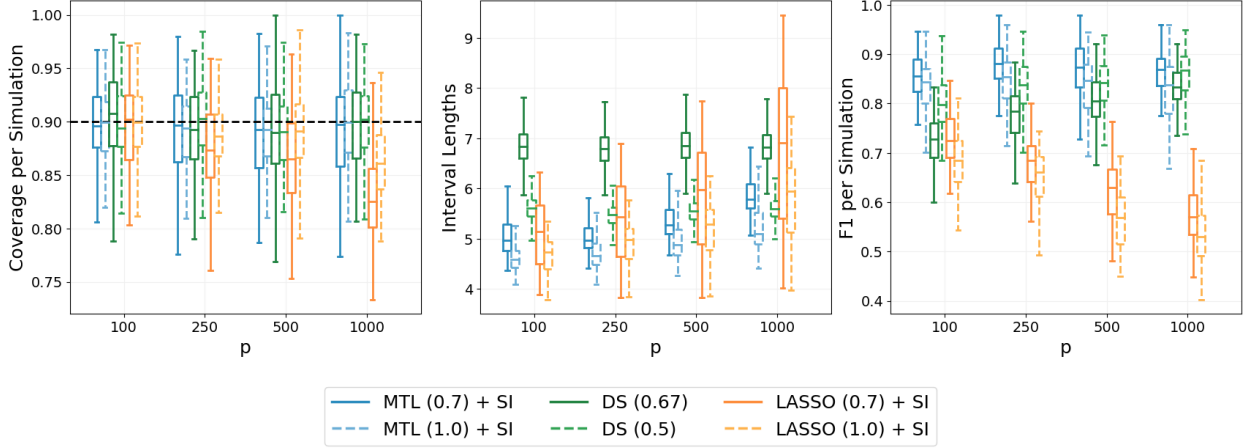


Figure 4: Results for 100 replications as a function of the number of predictors p , fixing task sparsity $s_T = 0$ and an average of 10 active predictors per task. Left: coverage; middle: interval length; right: F1 score.

Figure 2 shows the distribution of coverage, interval length, and the F1 score as we vary the task sparsity s_T from 0 to 0.6, holding s_G and p fixed. All methods consistently attain nominal or near-nominal coverage, regardless of task sparsity. Selective inference (MTL + SI) yields consistently shorter intervals than data splitting (DS), illustrating the benefit of using the whole sample rather than splitting. At all levels of task sparsity, but especially when there is more homogeneity in active predictors across tasks, MTL methods with selective inference also achieve better accuracy than single-task LASSO with selective inference as measured by the F1 score.

Figure 3 shows the same patterns continue to hold when we vary global sparsity while keeping task sparsity fixed. We only vary global sparsity between 0.8 and 0.95 because the problem becomes very easy for all methods at lower levels of global sparsity. MTL+ SI again outperforms other methods on both interval length and accuracy at all levels of global sparsity. We note, however, that the variance increases for all methods at larger levels of s_G .

Finally, Figure 4 shows the results as a function of the number of predictors p . To control the difficulty of the problem as p changes, we fix the average number of active predictors per task at 10, rather than specifying the fraction of active predictors. The average interval length for the selective inference methods grows slightly with p , reflecting the cost of conditioning upon additional information. Most overall patterns remain the same, with MTL + SI providing the best performance. The accuracy of LASSO + SI declines faster with p than that of other methods, indicating the growing cost of disregarding shared information. In summary, our simulation results show that there is variability in performance of all methods, but multi-task learning with selective inference achieves the nominal coverage in all settings and provides the best performance, on average, compared to either data splitting or single-task prediction.

5 Analysis of fMRI data from the ABCD study

The Adolescent Brain Cognitive Development (ABCD) study, discussed in the introduction, is one of the biggest efforts to date to track brain development of a large cohort of children (Jernigan et al., 2018). We consider data from the second release (the study is ongoing), applying the same inclusion/exclusion criteria as Sripada et al. (2021). This leaves resting-state fMRI scans for 5,937 subjects collected at 19 different research sites in the US. Resting-state fMRI is a form of imaging that captures spontaneous activation between functionally related areas of the brain while subjects are at rest in the scanner, in contrast to task-based fMRI, which images subjects performing a particular task. Research has shown that the resting-state connections across functional regions of the brain captured by resting state fMRI exhibit predictable and consistent patterns subject to inter-individual variation, leading to the discovery of the “functional connectome” (Biswal et al., 2010).

One of the main motivations for the ABCD study is understanding the relationship between brain connectivity, cognitive functioning, behavioral traits, and physical and mental health outcomes (Volkow et al., 2018; Luciana et al., 2018; Karcher and Barch, 2021). The battery of neurocognitive tests used in the ABCD study includes seven tasks from the NIH Toolbox for the Assessment of Neurologic and Behavioral Function that are designed to assess processing speed, working memory, episodic memory, attention, executive function, and language and reading abilities. Of the seven tasks, the Pattern Comparison Processing Speed Test (PC) measures rapid visual processing; the List Sorting Working Memory Test (LS) and the Picture Sequence Memory Test (PS) assess working and episodic memory, respectively; the Flanker Task (FT) tests executive function and attention; the Dimensional Change Card Sort Task (CS) assesses executive function and cognitive flexibility; and the Picture Vocabulary Test (PV) and the Oral Reading Recognition Test (RC) measure language and reading abilities (Gershon et al., 2013; Luciana et al., 2018). Apart from the NIH Toolbox, the ABCD study employs some other standard measures of cognition, including the Little Man Task (LMT), the Rey Auditory Verbal Learning Test (Ravlt), and an automated version of the Matrix Reasoning subtest from the Wechsler Intelligence Test for Children. Performance across tasks tends to be positively correlated across subjects, and thus multi-task learning is a natural approach to the problem. We will employ multi-task regression to understand the relationship between these cognitive measures and an individual’s functional connectome.

The predictors in our regression are derived by using resting-state fMRI scans to estimate the connections between 418 regions of interest (ROIs, or nodes) in the brain. These ROIs were identified based on the Gordon cortical parcellation (Gordon et al., 2016), augmented with additional subcortical and cerebellar atlases. The 418 ROIs are further classified into 15 functional groups (including “None”), ranging in size from 4 to 54 nodes. To assess the strength of connection between each

pair of nodes, the Pearson correlation coefficient is computed between the fMRI blood-oxygen-level-dependent (BOLD) signals at those nodes. [Sripada et al. \(2021\)](#) have provided us with the matrix of inter-node correlations they computed after pre-processing the fMRI time series data to correct for nuisance covariates, such as physiological noise and head motion, through a standard pipeline that includes FreeSurfer normalization, ICA-AROMA denoising, CompCor correction, and omission of high-motion frames. With 418 nodes, each scan corresponds to $418 \times 417/2 = 87,153$ features.

Resting-state fMRI data is complicated not only by the inherent dimensionality but also by a low signal-to-noise ratio, so the raw features are often replaced with the top principal component scores ([Cordes and Nandy, 2006](#)). We retain only the first 1,000 principal component scores computed from the correlations to use as features in multi-task learning. Previous work has shown that just the top several principal components are sufficient to capture most inter-individual variation in functional connectivity ([Sripada et al., 2019](#)) and successfully predict differences in higher-order cognition ([Sripada et al., 2020](#)), so we expect that the number of true signals will still be sparse among the first 1,000 principal components.

We identify the most relevant principal components for each task by standardizing the response variables and applying [Algorithm 1](#). Our method allows non-consecutive principal components to be selected as true signals, unlike other techniques for estimating the dimensionality of resting-state fMRI data proposed by [Cordes and Nandy \(2006\)](#) and references therein. Thus, our model selection procedure can capture low-variance directions that may still be highly predictive of cognitive functioning for at least a subset of the subjects. After identifying the relevant features for each task, we fit a linear model on these principal components to predict the subjects’ standardized scores and construct confidence intervals for the best linear coefficients using [Algorithm 2](#). We use a consistent plug-in estimator for the noise level, following the recommendation of [Tian and Taylor \(2018\)](#). Consistent with the empirical experiments, we report our findings for two different values of randomization variable along with two data splits of comparable size. For each method, we use 80% of the original data for model selection and inference, hold out another 10% for selecting the tuning parameter for the penalized multi-task regression by minimizing the MSE on this validation set, and keep the last 10% to use as test data.

In evaluating the performance of our multi-task methods on the ABCD study data, we consider both their predictive power and inferential quality. Following the convention in the neuroimaging literature ([Sripada et al., 2020, 2021](#)), we measure predictive performance through the so-called predictive r , the correlation between predictions and observed responses on test data. Our results, shown in [Table 2](#), indicate that multi-task learning has comparable predictive performance to the randomized LASSO, with slightly less variability in performance between tasks. The predictive correlations obtained are

	MTL + SI (0.7)	LASSO (0.7) + SI	MTL (1.0) + SI	LASSO (1.0) + SI
NIH Tlhx PV	0.47	0.51	0.48	0.51
NIH Tlhx FT	0.16	0.09	0.14	0.09
NIH Tlhx LS	0.33	0.28	0.33	0.25
NIH Tlhx CS	0.23	0.24	0.24	0.24
NIH Tlhx PC	0.13	0.10	0.12	0.09
NIH Tlhx PS	0.21	0.22	0.21	0.13
NIH Tlhx RC	0.31	0.33	0.33	0.34
Ravlt Short Delay	0.31	0.28	0.32	0.30
Ravlt Long Delay	0.27	0.23	0.26	0.25
Matrix Reasoning	0.28	0.30	0.28	0.31
LMT	0.24	0.22	0.24	0.20

Table 2: Predictive correlation on test data for selected models for the 11 tasks and the general score. The value in parentheses is the randomization variance.

consistent with the expectations of domain experts and previous findings; see [Sripada et al. \(2021\)](#).

While the predictive power of the randomized LASSO and MTL are comparable, the chosen models are quite different. MTL selects more similar models across tasks, identifying many PCs as being relevant to several different cognitive functions. Training all of the 11 tasks together thus seems to reduce noise and offer improved detection of shared signals. To more rigorously test the significance of the shared structure, we consider the similarity between the sets of significant features for each pair of tasks, where similarity is measured through the Jaccard index and significant features are those PCs with post-selection confidence intervals that do not contain zero. Figure 5 shows the Jaccard index for the sets of significant features, quantifying the similarity between each pair of models, separately for both the randomized LASSO and MTL. For MTL (0.7) + SI, the Jaccard index ranges from 0.24 to 0.54, reflecting significant common structure between any two of the 11 tasks. The mean pair-wise Jaccard index is 0.36, compared to 0.14 for LASSO (0.7) + SI. The results for a randomizer scale of 1.0 reveal a similar pattern and are thus omitted. In essence, post-selection inference seems to confirm the existence of the shared signals identified through MTL, suggesting that there may be similar neural underpinnings for various cognitive functions that can be best understood through a multi-task learning framework.

To assess the quality of inference for MTL, we compare our post-selection inference methods to data splitting, considering a) the overall properties of the intervals formed by each procedure and b) the properties of intervals for shared parameters. Figure 6 shows the results. Randomized procedures clearly produce shorter intervals overall than data splitting. As another measure of how useful the

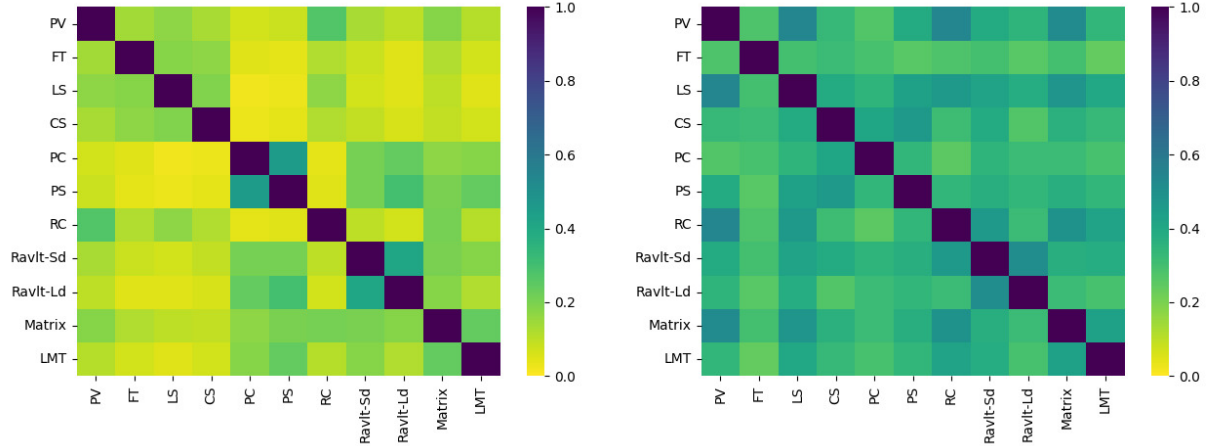


Figure 5: Pair-wise Jaccard index between sets of significant PCs. Left: LASSO (0.7) + SI. Right: MTL (0.7) + SI.

interval is, we consider the coefficient of variation, defined here as

$$\text{C.V.}(\hat{\beta}_{\mathbf{E},j}) = \frac{\text{S.E.}(\hat{\beta}_{\mathbf{E},j})}{|\hat{\beta}_{\mathbf{E},j}|}.$$

This measure also shows the advantage of selective inference methods, which yield shorter intervals relative to the estimated effect sizes. Finally, we compare the confidence intervals for parameters selected by both methods. Some of the selected predictors vary across methods since each method performs its own model selection; however, rough comparisons may still be possible when there is substantial overlap in the selected sets. The length ratios range roughly between 1.2 and 1.8, again demonstrating the advantage of selective inference. To put this in context, Table 3 reports the average number of features selected and further deemed significant across the 11 tasks for each method, as well as the average number of shared features between the comparable data splitting selective inference procedures. The overlap is significant, making the comparison more meaningful.

	rMSE	# selected	# significant
MTL (0.7) + SI	0.97	55.00	28.00
DS (0.67)	0.98	43.91	16.45
Common		28.82	14.27
MTL (1.0) + SI	0.97	68.18	32.91
DS (0.5)	0.97	74.27	22.63
Common		29.55	14.55

Table 3: Comparison of selected models, in average number of predictors per task

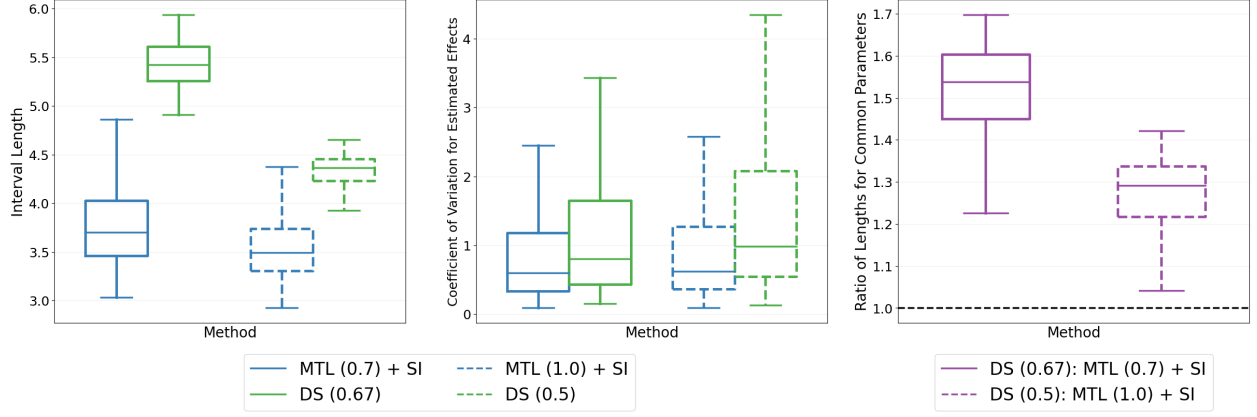


Figure 6: Evaluation of post-selection inference on ABCD data. Left: boxplots of interval lengths. Center: boxplots of coefficients of variation. Right: ratio of interval lengths for shared parameters.

In using resting-state fMRI data to predict phenotypes, principal components regression using only the top principal components can significantly enhance the signal-to-noise ratio and thus improve prediction. However, experts are ultimately interested in understanding the effects of the connectome, and thus it is useful to translate the results into the original 87,153-dimensional connectome feature space. Note that the mean structure for task k in the original feature space of dimension p can be represented as

$$X\beta^{(k)} = XAA'\beta^{(k)} = Z\theta^{(k)},$$

where A is the orthogonal matrix of eigenvectors for $X'X$, Z is the matrix of principal component scores, and $\theta^{(k)} = A'\beta^{(k)} \in \mathbb{R}^p$. To recover $\beta^{(k)}$, a potential plug-in estimator is

$$\hat{\beta}^{(k)} = A \begin{pmatrix} \hat{\theta}_{E_k}^{(k)} \\ 0 \end{pmatrix} = A_{E_k} \hat{\theta}_{E_k}^{(k)},$$

where $\hat{\theta}_{E_k}^{(k)} \in \mathbb{R}^{q_k}$ is the MLE for task k obtained from Algorithm 2. Although this estimator is only consistent for $\beta^{(k)}$ when $q_k = p$, we will use it to approximate $\beta^{(k)}$ as is typically done in ordinary principal components regression (Jolliffe, 2003).

The estimated multi-task coefficients in the original feature space reflect a significant degree of structure-sharing between tasks, consistent with our findings from the principal components regression. Figure 7 shows the cross-correlation matrix for the 11 coefficient vectors estimated with MTL (0.7) + SI, compared to the cross-correlation matrix for the 11 coefficient vectors estimated with LASSO (0.7) + SI. The mean pair-wise correlation for MTL (0.7) + SI is 0.54, while the mean pair-wise correlation for LASSO (0.7) + SI is 0.20. In the absence of any shared structure between tasks, the models

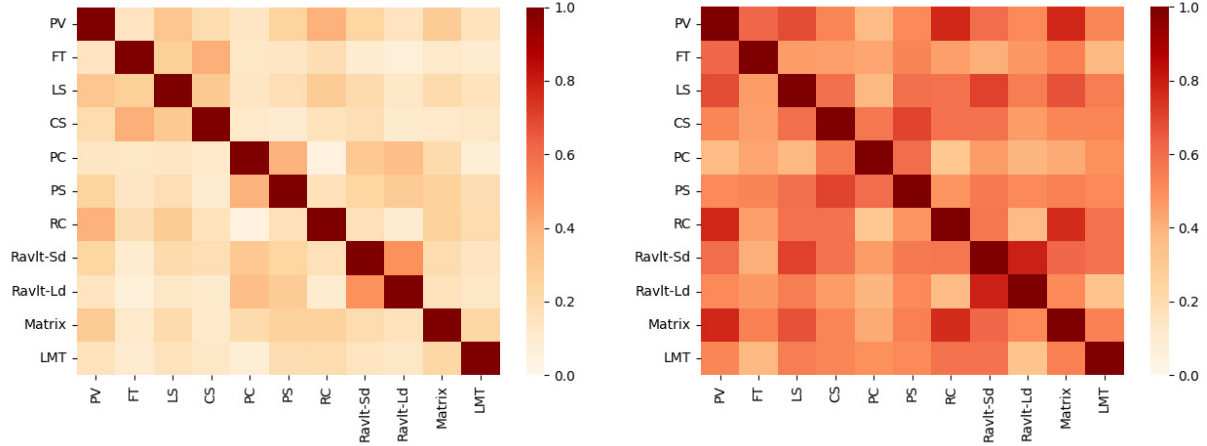


Figure 7: Cross-correlation matrices between the 11 estimated coefficient vectors in the original 87,153-dimensional feature space. Left: LASSO (0.7) + SI. Right: MTL (0.7) + SI.

identified through MTL would be expected to closely resemble those identified through single-task learning. Thus, the significant inter-task correlation between the MTL coefficients suggests that there are common signals across the tasks, and training the tasks jointly offers improved detection of those shared signals.

Given this strong evidence of shared structure across the 11 cognitive tasks, we next seek to further clarify and interpret the shared structure. More specifically, we visualize four tasks that are particularly important from the perspective of prior theory in psychology and neuroscience. Figure 8 shows the results for these four tasks from MTL projected back into the original feature space. The top row shows results for the picture vocabulary task and reading task, two tasks that implicate crystallized intelligence, i.e., intelligence rooted in determinate facts that are specifically trained through prior learning (Cattell, 1943; Horn and Noll, 1997). The bottom row shows results for the list working memory task and matrix reasoning task, which implicate fluid intelligence, i.e., intelligence rooted in manipulation of information and problem solving and that is largely independent of prior learning (Cattell, 1943; Gray et al., 2003; Blair, 2006).

There is notable similarity of connectivity patterns for the two crystallized tasks in the top row as well as for the two fluid tasks in the bottom row, broadly consistent with the crystallized/fluid model. A further question concerns the relationship between crystallized and fluid tasks. According to proponents of a “general factor” model, although crystallized tasks are superficially quite different from fluid tasks, and although they rely on cognitive skills acquired in quite different ways, there is nonetheless an underlying shared mental ability that drives performance in both kinds of tasks (Spearman, 1961; Humphreys, 1979; Carroll et al., 1993). Interestingly, we do in fact observe substantial shared structure

across the top and bottom row that provides some initial support for this general factor model.

Examining Figure 8, key connectivity motifs that are visible across the four tasks include: Stronger connections (both positive correlations and negative anti-correlations) within default mode network (DMN) and within visual network, as well as increased connectivity within cerebellum. There are also complex patterns of connectivity changes between networks, which especially implicate connections between frontoparietal network (FPN) and DMN; auditory network and somatomotor network; cinguloparietal (CP) network and ventral attention network; and retrosplenial (RSP) network and DMN. FPN is involved in flexible adaptive control (Cole et al., 2013), and a number of previous studies implicate it in executive functions and cognitive control (Cole and Schneider, 2007; Niendam et al., 2012), constructs closely related to the general factor of intelligence (Chen et al., 2019). DMN is involved in spontaneous thought (Andrews-Hanna et al., 2014) and semantic/conceptual representation (Wirth et al., 2011; Binder and Desai, 2011; Binder et al., 2009), capacities that likely facilitate abstraction and problem-solving. Cerebellum has been traditionally associated with coordination of movement (Spencer et al., 2005; Bastian, 2006), but there is growing recognition that it coordinates both external motor operations as well as internal mental operations, and thus it plays a critical role in supporting complex cognition (Schmahmann, 2019, 1996; Andreasen et al., 1999). CP and RSP are small networks that were identified relatively recently (Gordon et al., 2017), and their significance for higher cognitive functions requires further elucidation.

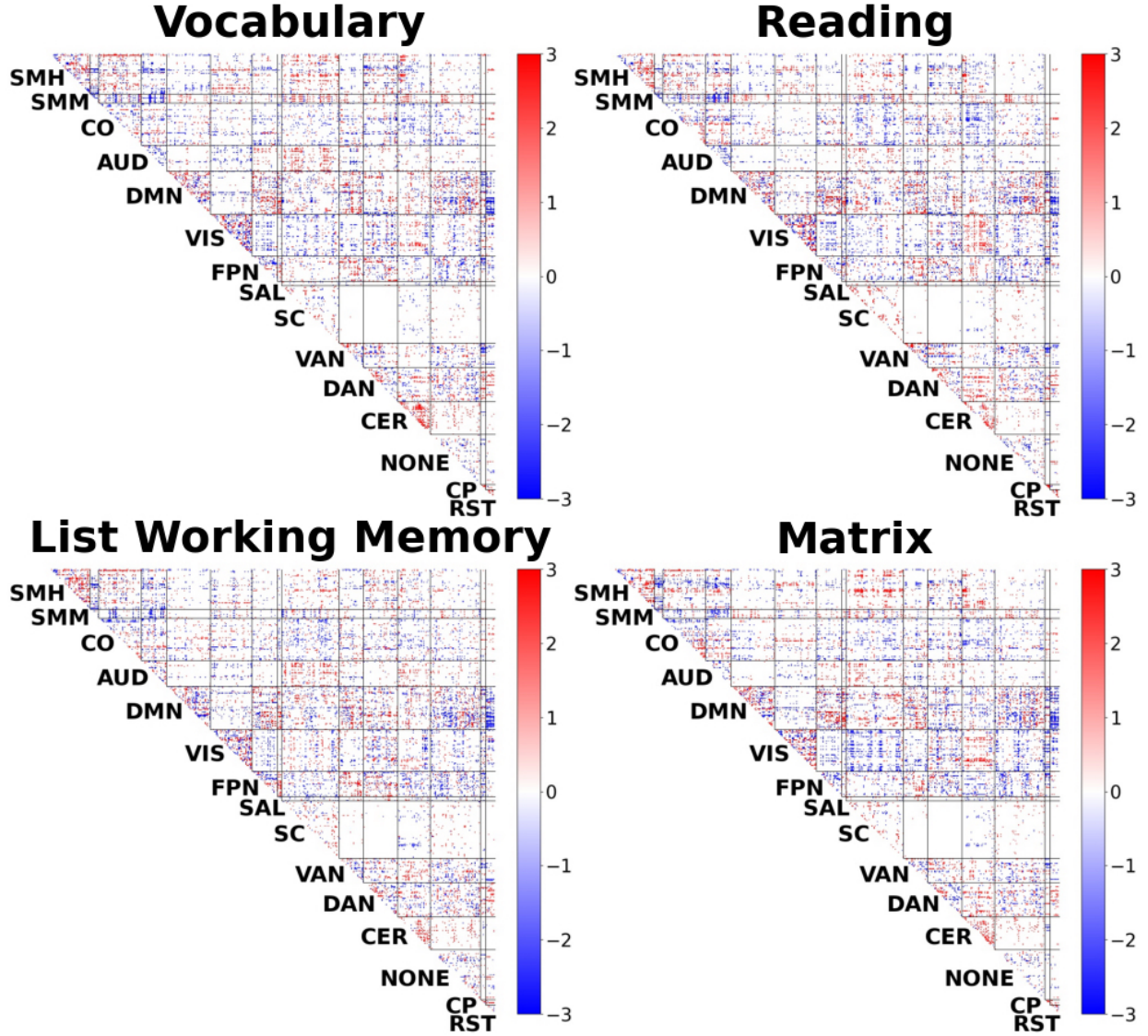


Figure 8: Estimated coefficients in the original feature space using MTL (0.7) + SI.

Figure 9 shows the same connectome-space visualization, using the coefficients from the randomized LASSO, for the two crystallized intelligence tasks (top row) and two fluid intelligence tasks (bottom row). In all four maps, patterns are less clumpy (more “salt-and-pepper”). In addition, there is less block structure wherein connectivity patterns follow the boundaries of our a priori parcellation that groups nodes into 15 network communities. While there is shared structure visible within rows, consistent with the crystallized/fluid model, and across rows, consistent with the general factor model, this shared structure is notably more muted compared to corresponding results from MTL.

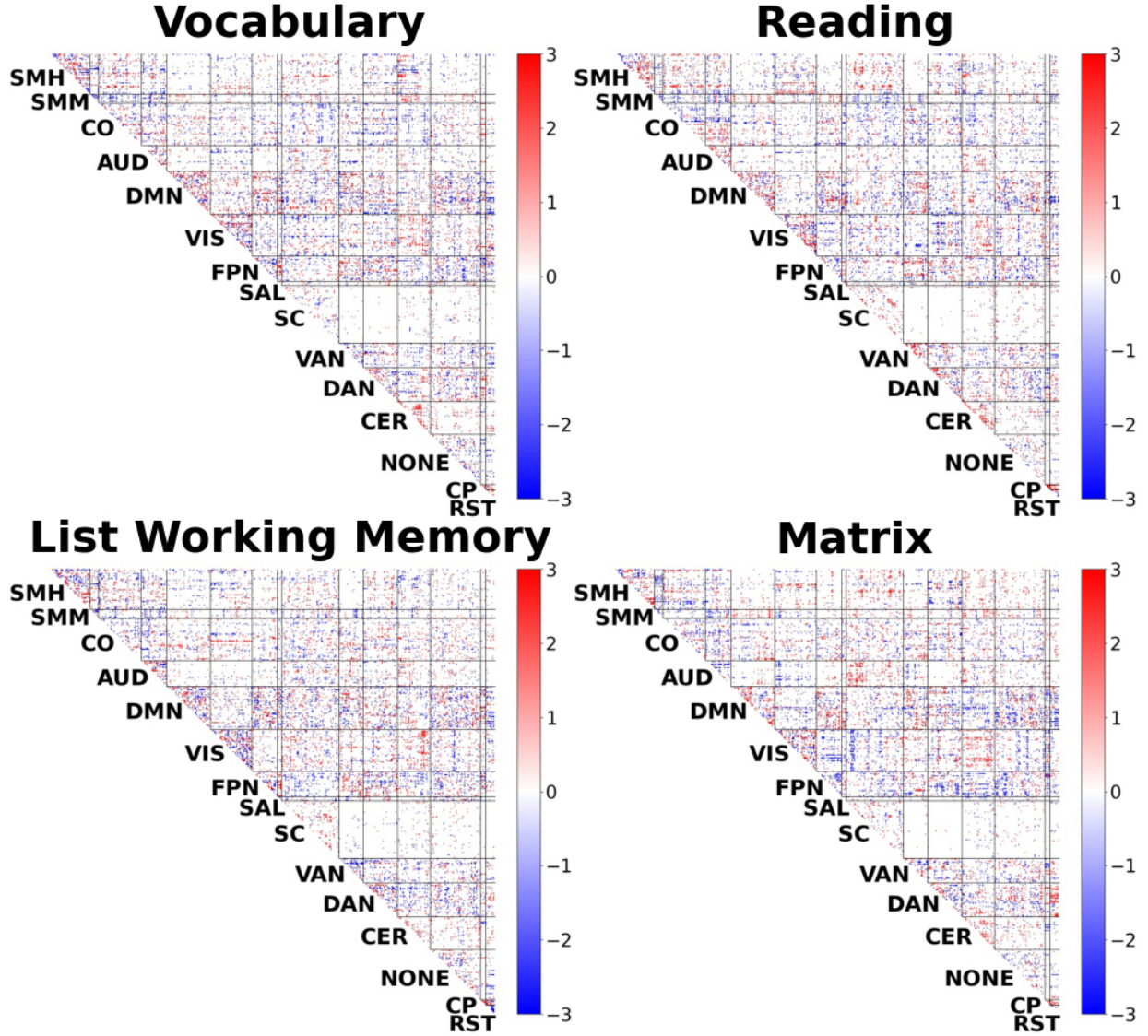


Figure 9: Estimated coefficients in the original feature space using LASSO (0.7) + SI.

Overall, we find compelling evidence for shared connectivity patterns across all eleven tasks, including across crystallized and fluid intelligence tasks. This result provides some support for the general factor model of cognitive abilities. Additionally, this shared structure is more readily identified and interpreted with MTL in comparison to single-task learning. Post-selective inference provides additional statistical reassurance that the shared structure we identified reflects real patterns in the data, rather than arising spuriously.

6 Discussion

To effectively analyze multi-task fMRI data, experts need interpretable models with valid inference that can facilitate interpretation and generate new hypotheses for further study. Our results on both synthetic data and the fMRI data from the ABCD study show that, first, multiple related tasks should be analyzed together whenever possible, and second, that post-selection inference provides a rigorous statistical approach to attaching uncertainty estimates to the results. Post-selection inference provided consistently better results than inference based on data splitting, demonstrating the additional power of randomization. The method is computationally efficient, with much less additional computational cost needed for inference after fitting the model relative to resampling-based inference or MCMC.

There are a variety of alternative ways to estimate the shared sparsity structure in MTL that could lead to different model selections, including one competing approach that uses the $\ell_{2,1}$ penalty to impose group-wise sparsity (Obozinski et al., 2006; Rao et al., 2013). The focus of our work is primarily on conducting valid inference for a class of plausible models, and some models and penalties are easier to work with than others. Our method is quite flexible, with many feasible extensions. For instance, our approach can be extended to models involving basis splines or kernel-weighted local polynomials.

7 Acknowledgments

We would like to thank Ji Zhu and Dan Kessler for their helpful feedback throughout the project; Qianhua Shan for guidance in accessing the ABCD dataset; Tian Xie and Qiang Chen for helping with simulations as part of their undergraduate research project; and Aman Taxali for helping to generate the connectome visualizations. S. Panigrahi’s research is supported in part by NSF grants: NSF-DMS 1951980 and NSF-DMS 2113342. N. Stewart is supported in part by NSF RTG grant 1646108 and a Rackham Science Award from the University of Michigan. C. Sripada and E. Levina received support for the research from an NIMH grant R01MH123458. E. Levina’s research is also supported in part by NSF grants 1916222 and 2052918.

References

- Andreasen, N. C., Nopoulos, P., O’Leary, D. S., Miller, D. D., Wassink, T., and Flaum, M. (1999). Defining the phenotype of schizophrenia: cognitive dysmetria and its neural mechanisms. *Biological psychiatry*, 46(7):908–920.
- Andrews-Hanna, J. R., Smallwood, J., and Spreng, R. N. (2014). The default network and self-generated thought: Component processes, dynamic control, and clinical relevance. *Annals of the new York Academy of Sciences*, 1316(1):29–52.

- Bastian, A. J. (2006). Learning to predict the future: the cerebellum adapts feedforward movement control. *Current opinion in neurobiology*, 16(6):645–649.
- Benjamini, Y. (2020). Selective inference: The silent killer of replicability.
- Bi, J., Xiong, T., Yu, S., Dundar, M., and Rao, R. (2008). An improved multi-task learning approach with applications in medical diagnosis. In *Joint European Conference on Machine Learning and Knowledge Discovery in Databases*, pages 117–132.
- Bi, N., Markovic, J., Xia, L., and Taylor, J. (2020). Inferactive data analysis. *Scandinavian Journal of Statistics*, 47(1):212–249.
- Binder, J. R. and Desai, R. H. (2011). The neurobiology of semantic memory. *Trends in cognitive sciences*, 15(11):527–536.
- Binder, J. R., Desai, R. H., Graves, W. W., and Conant, L. L. (2009). Where is the semantic system? A critical review and meta-analysis of 120 functional neuroimaging studies. *Cerebral cortex*, 19(12):2767–2796.
- Biswal, B. B., Mennes, M., Zuo, X.-N., Gohel, S., Kelly, C., Smith, S. M., Beckmann, C. F., Adelstein, J. S., Buckner, R. L., Colcombe, S., et al. (2010). Toward discovery science of human brain function. *Proceedings of the National Academy of Sciences*, 107(10):4734–4739.
- Blair, C. (2006). How similar are fluid cognition and general intelligence? A developmental neuroscience perspective on fluid cognition as an aspect of human cognitive ability. *Behavioral and Brain Sciences*, 29(2):109–125.
- Carroll, J. B. et al. (1993). *Human cognitive abilities: A survey of factor-analytic studies*. Number 1. Cambridge University Press.
- Cattell, R. B. (1943). The measurement of adult intelligence. *Psychological bulletin*, 40(3):153.
- Chen, Y., Spagna, A., Wu, T., Kim, T. H., Wu, Q., Chen, C., Wu, Y., and Fan, J. (2019). Testing a cognitive control model of human intelligence. *Scientific reports*, 9(1):1–17.
- Cole, M. W., Reynolds, J. R., Power, J. D., Repovs, G., Anticevic, A., and Braver, T. S. (2013). Multi-task connectivity reveals flexible hubs for adaptive task control. *Nature neuroscience*, 16(9):1348–1355.
- Cole, M. W. and Schneider, W. (2007). The cognitive control network: Integrated cortical regions with dissociable functions. *Neuroimage*, 37(1):343–360.

- Cordes, D. and Nandy, R. R. (2006). Estimation of the intrinsic dimensionality of fMRI data. *Neuroimage*, 29(1):145–154.
- Fithian, W., Sun, D., and Taylor, J. (2017). Optimal inference after model selection.
- Gershon, R. C., Wagster, M. V., Hendrie, H. C., Fox, N. A., Cook, K. F., and Nowinski, C. J. (2013). NIH Toolbox for Assessment of Neurological and Behavioral Function. *Neurology*, 80(11 Supplement 3):S2–S6.
- Goncalves, A., Ray, P., Soper, B., Widemann, D., Nygård, M., Nygård, J., and Sales, A. (2019). Bayesian multitask learning regression for heterogeneous patient cohorts. *Journal of Biomedical Informatics*, X(4):100059.
- Gordon, E. M., Laumann, T. O., Adeyemo, B., Gilmore, A. W., Nelson, S. M., Dosenbach, N. U., and Petersen, S. E. (2017). Individual-specific features of brain systems identified with resting state functional correlations. *Neuroimage*, 146:918–939.
- Gordon, E. M., Laumann, T. O., Adeyemo, B., Huckins, J. F., Kelley, W. M., and Petersen, S. E. (2016). Generation and evaluation of a cortical area parcellation from resting-state correlations. *Cerebral cortex*, 26(1):288–303.
- Gray, J. R., Chabris, C. F., and Braver, T. S. (2003). Neural mechanisms of general fluid intelligence. *Nature neuroscience*, 6(3):316–322.
- Guo, J., Levina, E., Michailidis, G., and Zhu, J. (2011). Joint estimation of multiple graphical models. *Biometrika*, 98(1):1–15.
- Hagler Jr, D. J., Hatton, S., Cornejo, M. D., Makowski, C., Fair, D. A., Dick, A. S., Sutherland, M. T., Casey, B., Barch, D. M., Harms, M. P., et al. (2019). Image processing and analysis methods for the Adolescent Brain Cognitive Development study. *Neuroimage*, 202:116091.
- Horn, J. L. and Noll, J. (1997). Human cognitive capabilities: Gf-Gc theory.
- Hu, D. and Zeng, L.-L. (2019). Multi-task learning of structural MRI for multi-site classification. *Pattern Analysis of the Human Connectome*, pages 205–226.
- Humphreys, L. G. (1979). The construct of general intelligence.
- Jernigan, T. L., Brown, S. A., and Dowling, G. J. (2018). The Adolescent Brain Cognitive Development study. *Journal of research on adolescence: the official journal of the Society for Research on Adolescence*, 28(1):154.

- Jolliffe, I. T. (2003). Principal Component Analysis. *Technometrics*, 45(3):276.
- Karcher, N. R. and Barch, D. M. (2021). The ABCD study: understanding the development of risk for mental and physical health outcomes. *Neuropsychopharmacology*, 46(1):131–142.
- Kivaranovic, D. and Leeb, H. (2018). Expected length of post-model-selection confidence intervals conditional on polyhedral constraints. *arXiv preprint arXiv:1803.01665*.
- Lee, J. D., Sun, D. L., Sun, Y., and Taylor, J. E. (2016). Exact post-selection inference with the lasso. *The Annals of Statistics*, 44(3):907–927.
- Liu, K., Markovic, J., and Tibshirani, R. (2018). More powerful post-selection inference, with application to the lasso. *arXiv preprint arXiv:1801.09037*.
- Lozano, A. and Swirszcz, G. (2012). Multi-level lasso for sparse multi-task regression. In *Proceedings of the 29th International Conference on Machine Learning*, pages 595–602.
- Luciana, M., Bjork, J., Nagel, B., Barch, D., Gonzalez, R., Nixon, S., and Banich, M. (2018). Adolescent neurocognitive development and impacts of substance use: Overview of the adolescent brain cognitive development (ABCD) baseline neurocognition battery. *Developmental cognitive neuroscience*, 32:67–79.
- Ma, Q., Zhang, T., Zanetti, M. V., Shen, H., Satterthwaite, T. D., Wolf, D. H., Gur, R. E., Fan, Y., Hu, D., Busatto, G. F., et al. (2018). Classification of multi-site MR images in the presence of heterogeneity using multi-task learning. *NeuroImage: Clinical*, 19:476–486.
- Niendam, T. A., Laird, A. R., Ray, K. L., Dean, Y. M., Glahn, D. C., and Carter, C. S. (2012). Meta-analytic evidence for a superordinate cognitive control network subserving diverse executive functions. *Cognitive, Affective, & Behavioral Neuroscience*, 12(2):241–268.
- Obozinski, G., Taskar, B., and Jordan, M. (2006). Multi-task feature selection. In *Technical report, Department of Statistics, University of California, Berkeley*.
- Panigrahi, S. (2018). Carving model-free inference. *arXiv preprint arXiv:1811.03142*.
- Panigrahi, S. and Taylor, J. (2022). Approximate selective inference via maximum likelihood. *Journal of the American Statistical Association*, *Forthcoming*.
- Panigrahi, S., Taylor, J., et al. (2018). Scalable methods for bayesian selective inference. *Electronic Journal of Statistics*, 12(2):2355–2400.

- Panigrahi, S., Taylor, J., and Weinstein, A. (2021). Integrative methods for post-selection inference under convex constraints. *Annals of Statistics*, 49(5):2803–2824.
- Rao, N., Cox, C., Nowak, R., and Rogers, T. (2013). Sparse overlapping sets lasso for multitask learning and its application to fMRI analysis. In *Advances in Neural Information Processing Systems* 26.
- Schmahmann, J. D. (1996). From movement to thought: anatomic substrates of the cerebellar contribution to cognitive processing. *Human brain mapping*, 4(3):174–198.
- Schmahmann, J. D. (2019). The cerebellum and cognition. *Neuroscience letters*, 688:62–75.
- Spearman, C. (1961). ” General Intelligence” Objectively Determined and Measured.
- Spencer, R., Ivry, R. B., and Zelaznik, H. N. (2005). Role of the cerebellum in movements: control of timing or movement transitions? *Experimental brain research*, 161(3):383–396.
- Sripada, C., Angstadt, M., Rutherford, S., Kessler, D., Kim, Y., Yee, M., and Levina, E. (2019). Basic units of inter-individual variation in resting state connectomes. *Scientific reports*, 9(1):1–12.
- Sripada, C., Angstadt, M., Taxali, A., Clark, D. A., Greathouse, T., Rutherford, S., Dickens, J. R., Shedden, K., Gard, A. M., Hyde, L. W., et al. (2021). Brain-wide functional connectivity patterns support general cognitive ability and mediate effects of socioeconomic status in youth. *Translational psychiatry*, 11(1):1–8.
- Sripada, C., Rutherford, S., Angstadt, M., Thompson, W. K., Luciana, M., Weigard, A., Hyde, L. H., and Heitzeg, M. (2020). Prediction of neurocognition in youth from resting state fMRI. *Molecular psychiatry*, 25(12):3413–3421.
- Suzumura, S., Nakagawa, K., Umez, Y., Tsuda, K., and Takeuchi, I. (2017). Selective inference for sparse high-order interaction models. In *International Conference on Machine Learning*, pages 3338–3347. PMLR.
- Tanizaki, K., Hashimoto, N., Inatsu, Y., Hontani, H., and Takeuchi, I. (2020). Computing valid p-values for image segmentation by selective inference. In *Proceedings of the IEEE/CVF Conference on Computer Vision and Pattern Recognition*, pages 9553–9562.
- Taylor, J. and Tibshirani, R. (2018). Post-selection inference for-penalized likelihood models. *Canadian Journal of Statistics*, 46(1):41–61.

- Tian, X. and Taylor, J. (2018). Selective inference with a randomized response. *The Annals of Statistics*, 46(2):679–710.
- Titsias, M. and Lázaro-Gredilla, M. (2011). Spike and slab variational inference for multi-task and multiple kernel learning. *Advances in neural information processing systems*, 24.
- Volkow, N. D., Koob, G. F., Croyle, R. T., Bianchi, D. W., Gordon, J. A., Koroshetz, W. J., Pérez-Stable, E. J., Riley, W. T., Bloch, M. H., Conway, K., et al. (2018). The conception of the ABCD study: From substance use to a broad NIH collaboration. *Developmental cognitive neuroscience*, 32:4–7.
- Wang, X., Bi, J., Sun, J., and Song, M. (2016). Multiplicative multitask feature learning. *The Journal of Machine Learning Research*, 17(1):2820–2852.
- Wirth, M., Jann, K., Dierks, T., Federspiel, A., Wiest, R., and Horn, H. (2011). Semantic memory involvement in the default mode network: a functional neuroimaging study using independent component analysis. *Neuroimage*, 54(4):3057–3066.
- Xiao, L., Stephen, J. M., Wilson, T. W., Calhoun, V. D., and Wang, Y.-P. (2019). A manifold regularized multi-task learning model for IQ prediction from two fMRI paradigms. *IEEE Transactions on Biomedical Engineering*, 67(3):796–806.
- Zhang, Y. and Yang, Q. (2021). A survey on multi-task learning. *IEEE Transactions on Knowledge and Data Engineering*.
- Zhao, Q. and Panigrahi, S. (2019). Selective inference for effect modification: An empirical investigation. *Observational Studies*, 5(2):131–140.
- Zhou, J., Liu, J., Narayan, V. A., Ye, J., Initiative, A. D. N., et al. (2013). Modeling disease progression via multi-task learning. *NeuroImage*, 78:233–248.
- Zou, H. and Li, R. (2008). One-step sparse estimates in nonconcave penalized likelihood models. *The Annals of Statistics*, 36(4):1509–1533.
- Zu, C., Jie, B., Liu, M., Chen, S., Shen, D., and Zhang, D. (2016). Label-aligned multi-task feature learning for multimodal classification of Alzheimer’s disease and mild cognitive impairment. *Brain imaging and behavior*, 10(4):1148–1159.

8 Appendix

A Proofs of Results in Section 3

Proof: Proof of Lemma 3.1. The proof follows immediately from the definition of \mathbf{V} , $\mathbf{\Gamma}$ and by noting that the constraints $b^{(k)} > 0$ for all $k \in [K]$ are equivalent to

$$\mathbf{V} > \mathbf{0}, \mathbf{\Gamma} - D\mathbf{V} > \mathbf{0}.$$

□

Proof: Proof of Theorem 3.2. Based on the independence between $\hat{\beta}_{\mathbf{E}}$, $\hat{\beta}_{\perp}$ and \mathbf{W} , the unconditional law for the corresponding variables is given by

$$\prod_{k=1}^K \rho \left(\hat{\beta}_{E_k}^{(k)}; \beta_{E_k}^{(k)}, \sigma_k^2 \cdot X_{E_k}^{(k)'} X_{E_k}^{(k)} \right) \rho \left(\hat{\beta}_{\perp}^{(k)}; \mathbf{0}, \Sigma_{\perp}^{(k)} \right) \rho \left(w^{(k)}; \mathbf{0}, \Omega^{(k)} \right),$$

treating E_k for $k \in [K]$ as fixed sets. Consider the change of variables

$$\mathbf{W} \xrightarrow{(\Pi_{\mathbf{X}'\mathbf{Y}} \circ \Psi_A)^{-1}} \begin{pmatrix} \mathbf{V} & \mathbf{\Gamma} & \mathbf{U} \end{pmatrix}, \quad (17)$$

formed by inverting the composition of $\Pi_{\mathbf{X}'\mathbf{Y}}$, defined in (11), and Ψ_A . Applying (17), we observe that the law of the variables $\hat{\beta}_{\mathbf{E}}$, $\hat{\beta}_{\perp}$, \mathbf{V} , $\mathbf{\Gamma}$ and \mathbf{U} is equal to

$$\begin{aligned} |J_{(\Pi_{\mathbf{X}'\mathbf{Y}} \circ \Psi_A)}| & \left\{ \prod_{k=1}^K \rho \left(\hat{\beta}_{E_k}^{(k)}; \beta_{E_k}^{(k)}, \sigma_k^2 \cdot X_{E_k}^{(k)'} X_{E_k}^{(k)} \right) \rho \left(\hat{\beta}_{\perp}^{(k)}; \mathbf{0}, \Sigma_{\perp}^{(k)} \right) \right\} \\ & \times \rho(\Pi_{\mathbf{X}'\mathbf{Y}} \circ \Psi_A(\mathbf{V}, \mathbf{\Gamma}, \mathbf{U}); \mathbf{0}, \mathbf{\Omega}), \end{aligned}$$

where we let $J_{(\Pi_{\mathbf{X}'\mathbf{Y}} \circ \Psi_A)}$ be the Jacobian for the change of variables mapping and $\mathbf{\Omega} \in \mathbb{R}^{Kp \times Kp}$ is the block diagonal matrix with the diagonal entries equal to $\Omega^{(k)} \in \mathbb{R}^{p \times p}$ for $k \in [K]$. To complete the details of the proof, we introduce some matrices. Let $\mathcal{A} = \begin{bmatrix} \mathcal{A}_1 & \mathcal{A}_2 \end{bmatrix}$. Note that

$$(\Pi_{\mathbf{X}'\mathbf{Y}} \circ \Psi_A)(\mathbf{V}, \mathbf{\Gamma}, \mathbf{U}) = \mathcal{C}_1 \hat{\beta}_{\mathbf{E}} + \mathcal{C}_2 \mathbf{V} + f(\mathbf{\Gamma}, \mathbf{U}; \hat{\beta}_{\perp})$$

where

$$\begin{aligned} \mathcal{C}_1 &= -\text{Diag} \left(X^{(1)'} X_{E_1}^{(1)}, \dots, X^{(K)'} X_{E_K}^{(K)} \right) \\ \mathcal{C}_0 &= -\mathcal{C}_1 + \epsilon \text{Diag} \left((\mathbf{I}_{q_1} \ 0)', \dots, (\mathbf{I}_{q_K} \ 0)' \right) \end{aligned}$$

$$\mathcal{C}_2 = \mathcal{C}_0 (\mathcal{A}_1 - \mathcal{A}_2 D), \text{ and}$$

$$f(\Gamma, \mathbf{U}; \hat{\beta}_\perp) = \text{Diag}(\Lambda) (\mathbf{S}' \ \mathbf{U}')' + \mathcal{C}_0 \mathcal{A}_2 \Gamma - \hat{\beta}_\perp.$$

Additionally, we define

$$\Delta^{-1} = \mathcal{C}_2' \Omega^{-1} \mathcal{C}_2; \quad P = -\Delta \mathcal{C}_2' \Omega^{-1} \mathcal{C}_1; \quad q = -\Delta \mathcal{C}_2' \Omega^{-1} f(\Gamma, \mathbf{U}; \hat{\beta}_\perp);$$

$$\Sigma^{-1} = \text{Diag} \left(\sigma_1^2 \cdot \left(X_{E_1}^{(1)'} X_{E_1}^{(1)} \right)^{-1}, \dots, \sigma_K^2 \cdot \left(X_{E_K}^{(K)'} X_{E_K}^{(K)} \right)^{-1} \right)^{-1} + \mathcal{C}_1' \Omega^{-1} \mathcal{C}_1 - P' \Delta^{-1} P;$$

$$L = \Sigma \text{Diag} \left(\sigma_1^2 \cdot \left(X_{E_1}^{(1)'} X_{E_1}^{(1)} \right)^{-1}, \dots, \sigma_K^2 \cdot \left(X_{E_K}^{(K)'} X_{E_K}^{(K)} \right)^{-1} \right)^{-1}; \text{ and}$$

$$m = \Sigma P' \Delta^{-1} q - \Sigma \mathcal{C}_1' \Omega^{-1} f(\Gamma, \mathbf{U}; \hat{\beta}_\perp).$$

Conditioning upon $\hat{\beta}_\perp$ and the event in (12), which we note is equivalent to

$$\left\{ \mathbf{V} > \mathbf{0}, \ \Gamma - D\mathbf{V} > 0, \ \hat{\Gamma} = \Gamma, \ \hat{\mathbf{U}} = \mathbf{U} \right\}$$

based on Lemma 3.1, the law for $\hat{\beta}_\mathbf{E}$ and \mathbf{V} is given up to a constant by

$$\left(\int \rho(\tilde{\beta}; L\beta_\mathbf{E} + m, \Sigma) \cdot \rho(\tilde{V}; P\tilde{\beta} + q, \Delta) \cdot 1(H\tilde{V} \geq g) \, d\tilde{V} d\tilde{\beta} \right)^{-1} \cdot \\ \rho(\hat{\beta}_\mathbf{E}; L\beta_\mathbf{E} + m, \Sigma) \cdot \rho(\mathbf{V}; P\hat{\beta}_\mathbf{E} + q, \Delta) \cdot 1(H\mathbf{V} \geq g).$$

Integrating over \mathbf{V} in the last display and noting that

$$\int_{\{\tilde{V}: H\tilde{V} \geq g\}} \rho(\tilde{V}; P\hat{\beta}_\mathbf{E} + q, \Delta) d\tilde{V}$$

is a constant free from the parameters $\beta_\mathbf{E}$ in our model, we complete the proof of the Theorem. \square

Proof: Proof of Theorem 3.3. Observe that the maximum likelihood estimate is obtained by maximizing the following objective with respect to $\beta_\mathbf{E}$:

$$\begin{aligned} \underset{\beta_\mathbf{E}}{\text{maximize}} \quad & \hat{\beta}_\mathbf{E}' \Sigma^{-1} (L\beta_\mathbf{E} + m) + \inf_{\tilde{\beta}, \tilde{V}} \left\{ \frac{1}{2} \tilde{\beta}' \Sigma^{-1} \tilde{\beta} - \tilde{\beta}' \Sigma^{-1} (L\beta_\mathbf{E} + m) \right. \\ & \left. + \frac{1}{2} (\tilde{V} - P\tilde{\beta} - q)' \Delta^{-1} (\tilde{V} - P\tilde{\beta} - q) + \phi_{H,g}(\tilde{V}) \right\}. \end{aligned} \quad (18)$$

Let

$$F^*(\zeta) = \sup_{\tilde{\beta}} \left\{ \tilde{\beta}'\zeta - \frac{1}{2}\tilde{\beta}'\Sigma^{-1}\tilde{\beta} - \inf_{\tilde{V}} \frac{1}{2}(\tilde{V} - P\tilde{\beta} - q)' \Delta^{-1}(\tilde{V} - P\tilde{\beta} - q) + \phi_{H,g}(\tilde{V}) \right\}$$

represent the convex conjugate for

$$F(\beta) = \frac{1}{2}\beta'\Sigma^{-1}\beta + \inf_{\tilde{V}} \frac{1}{2}(\tilde{V} - P\beta - q)' \Delta^{-1}(\tilde{V} - P\beta - q) + \phi_{H,g}(\tilde{V}).$$

Then, solving (18) is equivalent to the problem

$$\begin{aligned} & \underset{\beta_E}{\text{maximize}} \quad \hat{\beta}'_E \Sigma^{-1}(L\beta_E + m) - \sup_{\tilde{\beta}} \left\{ \tilde{\beta}'\Sigma^{-1}(L\beta_E + m) - \frac{1}{2}\tilde{\beta}'\Sigma^{-1}\tilde{\beta} \right. \\ & \quad \left. - \inf_{\tilde{V}} \frac{1}{2}(\tilde{V} - P\tilde{\beta} - q)' \Delta^{-1}(\tilde{V} - P\tilde{\beta} - q) + \phi_{H,g}(\tilde{V}) \right\} \\ & = \underset{\beta_E}{\text{maximize}} \quad \hat{\beta}'_E \Sigma^{-1}(L\beta_E + m) - F^*(\Sigma^{-1}(L\beta_E + m)). \end{aligned}$$

Using the identity $(\nabla F^*)^{-1} = \nabla F$ from convex analysis, we have

$$\begin{aligned} \Sigma^{-1}(L\hat{\beta}_E^{\text{MLE}} + m) &= (\nabla F^*)^{-1}(\hat{\beta}_E) \\ &= \Sigma^{-1}\hat{\beta}_E + \left(\frac{\partial}{\partial \beta} V(\beta) \Big|_{\beta=\hat{\beta}_E} - P \right)' \Delta^{-1}(\hat{V} - P\hat{\beta}_E - q) \\ & \quad + \left(\frac{\partial}{\partial \beta} V(\beta) \Big|_{\beta=\hat{\beta}_E} \right)' \nabla \phi_{H,g}(\hat{V}), \end{aligned}$$

where

$$V(\beta) = \underset{\tilde{V}}{\text{argmin}} \frac{1}{2}(\tilde{V} - P\beta - q)' \Delta^{-1}(\tilde{V} - P\beta - q) + \phi_{H,g}(\tilde{V}) \quad (19)$$

and $V(\hat{\beta}_E) = \hat{V}$, the optimizer defined in (16). By the definition of \hat{V} ,

$$\Delta^{-1}(\hat{V} - P\hat{\beta}_E - q) + \nabla \phi_{H,g}(\hat{V}) = 0,$$

and we can we derive the system of estimating equations

$$\hat{\beta}_E^{\text{MLE}} = L^{-1}\hat{\beta}_E + L^{-1}\Sigma P' \Delta^{-1}(P\hat{\beta}_E + q - \hat{V}) - L^{-1}m.$$

Using the curvature of the smooth approximate likelihood, we observe that the expression for the

observed Fisher information matrix is equal to

$$L' \Sigma^{-1} \nabla^2 F^*(\zeta) \Big|_{\zeta = \Sigma^{-1}(L \hat{\beta}_{\mathbf{E}}^{\text{MLE}} + m)} \Sigma^{-1} L = L' \Sigma^{-1} \frac{\partial}{\partial \zeta} \beta^*(\zeta) \Big|_{\zeta = \Sigma^{-1}(L \hat{\beta}_{\mathbf{E}}^{\text{MLE}} + m)} \Sigma^{-1} L.$$

Here, ∇^2 denotes the Hessian matrix, and

$$\beta^*(\zeta) = \underset{\tilde{\beta}}{\text{argsup}} \left\{ \tilde{\beta}' \zeta - \frac{1}{2} \tilde{\beta}' \Sigma^{-1} \tilde{\beta} - \inf_{\tilde{V}} \frac{1}{2} (\tilde{V} - P \tilde{\beta} - \mathbf{q})' \Delta^{-1} (\tilde{V} - P \tilde{\beta} - \mathbf{q}) + \phi_{H,g}(\tilde{V}) \right\}. \quad (20)$$

From the K.K.T. conditions of optimality for (20),

$$\zeta = (\Sigma^{-1} + P' \Delta^{-1} P) \beta^*(\zeta) - P' \Delta^{-1} (V(\beta^*(\zeta)) - q),$$

which leads to noting

$$\frac{\partial}{\partial \beta} V(\beta) \Big|_{\beta = \beta^*(\zeta)} = (\Delta^{-1} + \nabla^2 \phi_{H,g}(V(\beta^*(\zeta))))^{-1} \Delta^{-1} P,$$

and

$$\begin{aligned} \frac{\partial}{\partial \zeta} \beta^*(\zeta) \Big|_{\zeta = \zeta_0} &= \left(\Sigma^{-1} + P' \Delta^{-1} P - P' \Delta^{-1} \frac{\partial}{\partial \beta} V(\beta) \Big|_{\beta = \beta^*(\zeta)} \right)^{-1} \\ &= \left(\Sigma^{-1} + P' \Delta^{-1} P - P' \Delta^{-1} (\Delta^{-1} + \nabla^2 \phi_{H,g}(V(\beta^*(\zeta_0))))^{-1} \Delta^{-1} P \right)^{-1}. \end{aligned}$$

Using, once again, the K.K.T. conditions of optimality for (20), we observe that

$$\beta^* \left(\Sigma^{-1} (L \hat{\beta}_{\mathbf{E}}^{\text{MLE}} + m) \right) = \hat{\beta}_{\mathbf{E}}.$$

Plugging

$$\frac{\partial}{\partial \zeta} \beta^*(\zeta) \Big|_{\zeta = \Sigma^{-1}(L \hat{\beta}_{\mathbf{E}}^{\text{MLE}} + m)}$$

into the expression for the observed Fisher information, we obtain the expression for the inverse information matrix:

$$\hat{\mathbf{I}}^{-1} = \mathbf{L}^{-1} \Sigma L'^{-1} + L^{-1} \Sigma \left(P' \Delta^{-1} P - P' \Delta^{-1} (\Delta^{-1} + \nabla^2 \phi_{H,g}(\hat{\mathbf{V}}))^{-1} \Delta^{-1} P \right) \Sigma L'^{-1}.$$

□

B Impracticality of Existing Conditional Prescription in Multi-Task Setting

In this section, we show in detail why the existing conditional prescription for other ℓ_1 -regularized algorithms after conditioning on the event in (10) does not lead to tractable inference. Given a stationary point (\mathbf{B}, \mathbf{U}) defined through the K.K.T. mapping in (11), we immediately note the following equivalence

$$\widehat{\mathbf{E}} = \mathbf{E}, \widehat{\mathbf{S}} = \mathbf{S} \equiv b^{(k)} > 0, \|u^{(k)}\|_\infty < 1 \text{ for all } k \in [K]. \quad (21)$$

The alternative characterization of the selection event through the K.K.T. mapping is directly analogous to the characterization used previously in conducting post-selection inference for the single-task LASSO. From here, the stationary mapping suggests a change of variables that may be useful in deriving a joint density function for the response and randomization variables. Proposition 1 provides us an expression for the Jacobian associated with the change of variables, and Proposition 2 describes the resulting selection-adjusted likelihood using the marginal law of the response vectors for the K tasks. Let $Q = \text{Diag}(Q^{(1,1)}, \dots, Q^{(K,K)})$, where the block matrices $Q^{(k,k)} \in \mathbb{R}^{p-q_k \times p-q_k}$ have columns given by

$$Q_{\cdot, \tilde{j}_k}^{(k,k)} = \Lambda_{\tilde{j}_k}^{(k)} \cdot \mathbf{e}_{\tilde{j}_k} \quad \text{for } j \in -E_k$$

Here, $\mathbf{e}_{\tilde{j}_k} \in \mathbb{R}^{q_k}$ is the standard basis vector whose \tilde{j}_k^{th} component is one, and all other components are zero. Let

$$R = \begin{pmatrix} R^{(1,1)} & \dots & R^{(1,K)} \\ \vdots & \ddots & \vdots \\ R^{(K,1)} & \dots & R^{(K,K)} \end{pmatrix},$$

where the block matrices $R^{(k,k')} \in \mathbb{R}^{q_k \times q_{k'}}$ are defined column-wise as

$$R_{\cdot, \tilde{j}_{k'}}^{(k,k')} = \begin{cases} -\left(\frac{1}{2}\lambda s_{\tilde{j}_k}^{(k)} \Gamma^{(j)}^{-\frac{3}{2}} s_{\tilde{j}_{k'}}^{(k')}\right) \cdot \mathbf{e}_{\tilde{j}_{k'}} & \text{if } j \in E_k \text{ and } \Lambda_{\tilde{j}_k}^{(k)} > \lambda_0 \\ 0 & \text{otherwise} \end{cases} \quad \text{for } j \in E_{k'}.$$

Finally, let

$$T = \text{Diag} \left((X_{E_1}^{(1)})' X_{E_1}^{(1)} + \epsilon \cdot \mathbf{I}_{q_1} \quad (X_{E_2}^{(2)})' X_{E_2}^{(2)} + \epsilon \cdot \mathbf{I}_{q_2} \quad \dots \quad (X_{E_K}^{(K)})' X_{E_K}^{(K)} + \epsilon \cdot \mathbf{I}_{q_K} \right) \cdot \text{Diag}(\mathbf{S}).$$

Proposition 1 Consider a change of variables $\mathbf{W} \xrightarrow{\Pi_{\mathbf{X}'\mathbf{Y}}^{-1}} (\mathbf{B} \quad \mathbf{U})$ where

$$\mathbf{W} = \Pi_{\mathbf{X}'\mathbf{Y}} (\mathbf{B} \quad \mathbf{U}) := \begin{pmatrix} \pi^{(1)}(b^{(1)}, u^{(1)}) & \pi^{(2)}(b^{(2)}, u^{(2)}) & \dots & \pi^{(K)}(b^{(K)}, u^{(K)}) \end{pmatrix}$$

and such that $\pi^{(k)}(\cdot)$ is defined according to (11). The Jacobian determinant associated with the above change of variables is given by

$$|J_{\Pi_{\mathbf{X}'\mathbf{Y}}}(\mathbf{B}, \mathbf{U})| = \det(Q) \det(R + T).$$

Proof: Proof of Proposition 1. We note that the Jacobian for the change of variables mapping $J_{\Pi_{\mathbf{X}'\mathbf{Y}}}$ is the determinant in absolute value for the following matrix

$$= \begin{bmatrix} \frac{\partial \pi^{(1)}}{\partial(b^{(1)}, u^{(1)})} & \frac{\partial \pi^{(1)}}{\partial(b^{(2)}, u^{(2)})} & \cdots & \frac{\partial \pi^{(1)}}{\partial(b^{(K)}, u^{(K)})} \\ \frac{\partial \pi^{(2)}}{\partial(b^{(1)}, u^{(1)})} & \frac{\partial \pi^{(2)}}{\partial(b^{(2)}, u^{(2)})} & \cdots & \frac{\partial \pi^{(2)}}{\partial(b^{(K)}, u^{(K)})} \\ \vdots & \ddots & & \vdots \\ \frac{\partial \pi^{(K)}}{\partial(b^{(1)}, u^{(1)})} & \frac{\partial \pi^{(K)}}{\partial(b^{(2)}, u^{(2)})} & \cdots & \frac{\partial \pi^{(K)}}{\partial(b^{(K)}, u^{(K)})} \end{bmatrix} \begin{bmatrix} \frac{\partial \omega_{E_1}^{(1)}}{\partial b^{(1)}} & \frac{\partial \omega_{E_1}^{(1)}}{\partial u^{(1)}} & \frac{\partial \omega_{E_1}^{(1)}}{\partial b^{(2)}} & \frac{\partial \omega_{E_1}^{(1)}}{\partial u^{(2)}} & \cdots & \frac{\partial \omega_{E_1}^{(1)}}{\partial b^{(K)}} & \frac{\partial \omega_{E_1}^{(1)}}{\partial u^{(K)}} \\ \frac{\partial \omega_{-E_1}^{(1)}}{\partial b^{(1)}} & \frac{\partial \omega_{-E_1}^{(1)}}{\partial u^{(1)}} & \frac{\partial \omega_{-E_1}^{(1)}}{\partial b^{(2)}} & \frac{\partial \omega_{-E_1}^{(1)}}{\partial u^{(2)}} & \cdots & \frac{\partial \omega_{-E_1}^{(1)}}{\partial b^{(K)}} & \frac{\partial \omega_{-E_1}^{(1)}}{\partial u^{(K)}} \\ \vdots & \ddots & & \ddots & & \vdots & \vdots \\ \frac{\partial \omega_{E_K}^{(K)}}{\partial b^{(1)}} & \frac{\partial \omega_{E_K}^{(K)}}{\partial u^{(1)}} & \frac{\partial \omega_{E_K}^{(K)}}{\partial b^{(2)}} & \frac{\partial \omega_{E_K}^{(K)}}{\partial u^{(2)}} & \cdots & \frac{\partial \omega_{E_K}^{(K)}}{\partial b^{(K)}} & \frac{\partial \omega_{E_K}^{(K)}}{\partial u^{(K)}} \\ \frac{\partial \omega_{-E_K}^{(K)}}{\partial b^{(1)}} & \frac{\partial \omega_{-E_K}^{(K)}}{\partial u^{(1)}} & \frac{\partial \omega_{-E_K}^{(K)}}{\partial b^{(2)}} & \frac{\partial \omega_{-E_K}^{(K)}}{\partial u^{(2)}} & \cdots & \frac{\partial \omega_{-E_K}^{(K)}}{\partial b^{(K)}} & \frac{\partial \omega_{-E_K}^{(K)}}{\partial u^{(K)}} \end{bmatrix}.$$

Noting in the above display $\frac{\partial \omega_{E_k}^{(k)}}{\partial u^{(k)}} = 0$ and $\frac{\partial \omega_{E_k}^{(k)}}{\partial u^{(k')}} = 0$ and $\frac{\partial \omega_{-E_k}^{(k)}}{\partial u^{(k')}} = 0$ for all $k' \neq k$, the above Jacobian equals

$$\begin{bmatrix} \frac{\partial \omega_{E_1}^{(1)}}{\partial b^{(1)}} & 0 & \frac{\partial \omega_{E_1}^{(1)}}{\partial b^{(2)}} & 0 & \cdots & \frac{\partial \omega_{E_1}^{(1)}}{\partial b^{(K)}} & 0 \\ \frac{\partial \omega_{-E_1}^{(1)}}{\partial b^{(1)}} & \frac{\partial \omega_{-E_1}^{(1)}}{\partial u^{(1)}} & \frac{\partial \omega_{-E_1}^{(1)}}{\partial b^{(2)}} & 0 & \cdots & \frac{\partial \omega_{-E_1}^{(1)}}{\partial b^{(K)}} & 0 \\ \vdots & & \ddots & & & \vdots & \vdots \\ \frac{\partial \omega_{E_K}^{(K)}}{\partial b^{(1)}} & 0 & \frac{\partial \omega_{E_K}^{(K)}}{\partial b^{(2)}} & 0 & \cdots & \frac{\partial \omega_{E_K}^{(K)}}{\partial b^{(K)}} & 0 \\ \frac{\partial \omega_{-E_K}^{(K)}}{\partial b^{(1)}} & 0 & \frac{\partial \omega_{-E_K}^{(K)}}{\partial b^{(2)}} & 0 & \cdots & \frac{\partial \omega_{-E_K}^{(K)}}{\partial b^{(K)}} & \frac{\partial \omega_{-E_K}^{(K)}}{\partial u^{(K)}} \end{bmatrix} \quad (22)$$

which further equals in absolute value the determinant of $\begin{bmatrix} M_1 & \mathbf{0} \\ M_2 & Q \end{bmatrix}$ where

$$M_1 = \begin{bmatrix} \frac{\partial \omega_{E_1}^{(1)}}{\partial b^{(1)}} & \frac{\partial \omega_{E_1}^{(1)}}{\partial b^{(2)}} & \cdots & \frac{\partial \omega_{E_1}^{(1)}}{\partial b^{(K)}} \\ \frac{\partial \omega_{E_2}^{(2)}}{\partial b^{(1)}} & \frac{\partial \omega_{E_2}^{(2)}}{\partial b^{(2)}} & \cdots & \frac{\partial \omega_{E_2}^{(2)}}{\partial b^{(K)}} \\ \vdots & \ddots & & \vdots \\ \frac{\partial \omega_{E_K}^{(K)}}{\partial b^{(1)}} & \frac{\partial \omega_{E_K}^{(K)}}{\partial b^{(2)}} & \cdots & \frac{\partial \omega_{E_K}^{(K)}}{\partial b^{(K)}} \end{bmatrix}, M_2 = \begin{bmatrix} \frac{\partial \omega_{-E_1}^{(1)}}{\partial b^{(1)}} & \frac{\partial \omega_{-E_1}^{(1)}}{\partial b^{(2)}} & \cdots & \frac{\partial \omega_{-E_1}^{(1)}}{\partial b^{(K)}} \\ \frac{\partial \omega_{-E_2}^{(2)}}{\partial b^{(1)}} & \frac{\partial \omega_{-E_2}^{(2)}}{\partial b^{(2)}} & \cdots & \frac{\partial \omega_{-E_2}^{(2)}}{\partial b^{(K)}} \\ \vdots & \ddots & & \vdots \\ \frac{\partial \omega_{-E_K}^{(K)}}{\partial b^{(1)}} & \frac{\partial \omega_{-E_K}^{(K)}}{\partial b^{(2)}} & \cdots & \frac{\partial \omega_{-E_K}^{(K)}}{\partial b^{(K)}} \end{bmatrix}, \text{ and}$$

$$Q = \text{Diag} \left(\frac{\partial \omega_{-E_1}^{(1)}}{\partial u^{(1)}}, \frac{\partial \omega_{-E_2}^{(2)}}{\partial u^{(2)}}, \dots, \frac{\partial \omega_{-E_K}^{(K)}}{\partial u^{(K)}} \right).$$

Observe $M_1 = R + T$, because

$$\frac{\partial \omega_{E_k}^{(k)}}{\partial b^{(k)}} = X_{E_k}^{(k)'} X_{E_k}^{(k)} + \epsilon \cdot \mathbf{I}_{n_k} + R^{(k,k)}, \quad \frac{\partial \omega_{E_k}^{(k)}}{\partial b^{(k')}} = R^{(k,k')} \text{ for } k \neq k'.$$

Using the block diagonal structure of (22), it follows that $|J_{\Pi_{\mathbf{X}'\mathbf{Y}}}(\mathbf{B}, \mathbf{U})| = \det(Q) \det(R + T)$. \square

Proposition 2 Suppose we observe the event (10) after solving (7). Fixing the set

$$\mathcal{O} = \left\{ (\tilde{Y}, \tilde{B}, \tilde{U}) : \tilde{b}^{(k)} > \mathbf{0}, \|\tilde{u}^{(k)}\|_\infty < 1 \text{ for all } k \in [K] \right\},$$

we let

$$\begin{aligned} \mathcal{N}_{\mathcal{O}}(\beta_{\mathbf{E}}) &:= \int_{\mathcal{O}} \left| J_{\Pi_{\mathbf{X}'\mathbf{Y}}}(\tilde{B}, \tilde{U}) \right| \cdot \prod_{k=1}^K \rho \left(\tilde{y}^{(k)}; X_{E_k}^{(k)} \beta_{E_k}^{(k)}, \sigma_k^2 \cdot \mathbf{I}_{n_k} \right) \\ &\quad \times \exp \left(-\frac{1}{2} \sum_{k=1}^K (\pi^{(k)}(\tilde{b}^{(k)}, \tilde{u}^{(k)}))' \Omega^{(k)-1} \pi^{(k)}(\tilde{b}^{(k)}, \tilde{u}^{(k)}) \right) d\tilde{B} d\tilde{U} d\tilde{Y}. \end{aligned}$$

Under the model in (9), the likelihood obtained from the law of \mathbf{Y} conditional upon (10) is given up to a constant by

$$(\mathcal{N}_{\mathcal{O}}(\beta_{\mathbf{E}}))^{-1} \prod_{k=1}^K \rho \left(y^{(k)}; X_{E_k}^{(k)} \beta_{E_k}^{(k)}, \sigma_k^2 \cdot \mathbf{I}_{n_k} \right).$$

Proof: Proof of Proposition 2. Let \mathcal{L} be the set of realizations of the responses and randomization variables that result in observing (10), that is

$$\mathcal{L} = \left\{ (\mathbf{Y}, \mathbf{W}) : \hat{\mathbf{E}}(\mathbf{Y}, \mathbf{W}) = \mathbf{E}, \hat{\mathbf{S}}(\mathbf{Y}, \mathbf{W}) = \mathbf{S} \right\}.$$

We note that the joint law of \mathbf{Y} , \mathbf{W} after conditioning out this observed event from (10) is obtained by truncating their unconditional Gaussian law and is given by:

$$\frac{\left\{ \prod_{k=1}^K \rho \left(y^{(k)}; X_{E_k}^{(k)} \beta_{E_k}^{(k)}, \sigma_k^2 \cdot \mathbf{I}_{n_k} \right) \cdot \rho(\omega^{(k)}; \mathbf{0}, \Omega^{(k)}) \right\} \cdot 1_{\mathcal{L}}(\mathbf{Y}, \mathbf{W})}{\int \left\{ \prod_{k=1}^K \rho \left(\tilde{y}^{(k)}; X_{E_k}^{(k)} \beta_{E_k}^{(k)}, \sigma_k^2 \cdot \mathbf{I}_{n_k} \right) \cdot \rho(\tilde{\omega}^{(k)}; \mathbf{0}, \Omega^{(k)}) \right\} \cdot 1_{\mathcal{L}}(\tilde{\mathbf{Y}}, \tilde{\mathbf{W}}) d\tilde{\mathbf{W}} d\tilde{\mathbf{Y}}}.$$

Using the change of variables mapping

$$\mathbf{W} = \Pi_{\mathbf{X}'\mathbf{Y}} \begin{pmatrix} \mathbf{B} & \mathbf{U} \end{pmatrix} = \begin{pmatrix} \pi^{(1)}(b^{(1)}, u^{(1)}) & \pi^{(2)}(b^{(2)}, u^{(2)}) & \dots & \pi^{(K)}(b^{(K)}, u^{(K)}) \end{pmatrix}$$

defined in (11), the conditional law for \mathbf{Y} , \mathbf{B} and \mathbf{U} is equal to

$$\begin{aligned} & \mathcal{N}_{\mathcal{O}}(\beta_{\mathbf{E}})^{-1} \left| \left(J_{\Pi_{\mathbf{X}'\mathbf{Y}}}(\mathbf{B}, \mathbf{U}) \right) \right| \prod_{k=1}^K \rho \left(y^{(k)}; X_{E_k}^{(k)} \beta_{E_k}^{(k)}, \sigma_k^2 \cdot \mathbf{I}_{n_k} \right) \\ & \cdot \exp \left(- \frac{1}{2} \sum_{k=1}^K (\pi^{(k)}(b^{(k)}, u^{(k)}))' \Omega^{(k)-1} \pi^{(k)}(b^{(k)}, u^{(k)}) \right) 1_{\{b^{(k)} > \mathbf{0}, \|u^{(k)}\|_{\infty} < 1 \text{ for } k \in [K]\}}(\mathbf{B}, \mathbf{U}), \end{aligned}$$

where we have used the equivalence of

$$\hat{\mathbf{E}}(\mathbf{Y}, \mathbf{W}) = \mathbf{E}, \quad \hat{\mathbf{S}}(\mathbf{Y}, \mathbf{W}) = \mathbf{S}$$

to the following constraints

$$b^{(k)} > \mathbf{0}, \|u^{(k)}\|_{\infty} < 1 \text{ for all } k \text{ in } \{1, 2, \dots, K\}.$$

Ignoring constants in $\beta_{\mathbf{E}}$ in the above expression, we deduce the claim in the Proposition. \square

The adjusted likelihood for this conditional prescription, seemingly a first-line recourse for post-selection inference, does not lend itself towards tractable estimating equations. Note that there is no clear method to compute the MLE given the following system of estimating equations:

$$\frac{\partial}{\partial \beta_{E_k}^{(k)}} \log \mathcal{N}_{\mathcal{O}}(\beta_{\mathbf{E}}) \Big|_{\hat{\beta}_{\mathbf{E}}^{\text{MLE}}} = \frac{1}{\sigma_k^2} X_{E_k}^{(k)'} \left(y^{(k)} - X_{E_k}^{(k)} \beta_{E_k}^{(k)} \right) \Big|_{\hat{\beta}_{\mathbf{E}}^{\text{MLE}}} \quad \text{for } k \in [K]$$

The absence of closed-form expressions for the partial derivatives of the Jacobian $J_{\Pi_{\mathbf{X}'\mathbf{Y}}}(\cdot)$ and the normalizing constant $\mathcal{N}_{\mathcal{O}}(\beta_{\mathbf{E}})$ poses a substantial obstacle in solving these equations. An attempt instead to numerically integrate out $Kp + N$ variables in the derivatives of the normalizing constant will turn out to be quite futile from an angle of computing efficiency.